AD-A095 865 ILLINOIS UNIV AT URBANA FUSION STUDIES LAB F/G 20/9
RESTRIKE PARTICLE BEAM EXPERIMENTS ON A DENSE PLASMA FOCUS.(U)
NOV 80 G GERDIN AFOSR-79-0121
UNCLASSIFIED AFOSR-TR-81-0184 NL

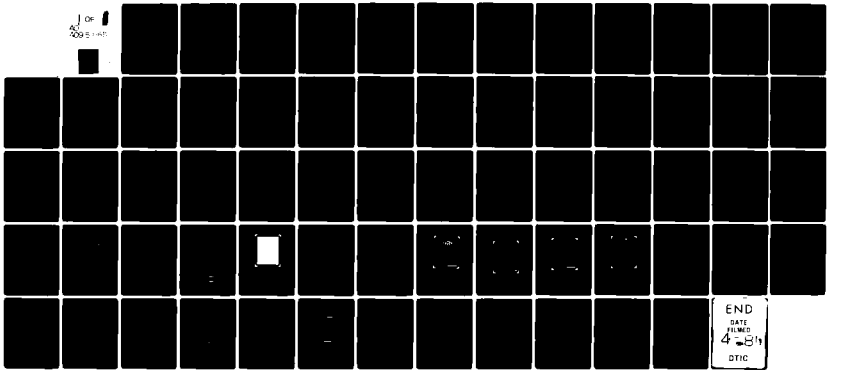

UNCLASSIFIED LEVEL II

SECURITY CLASSIFICATION OF THIS PAGE (When Data Entered)

REPORT DOCUMENTATION PAGE

READ INSTRUCTIONS BEFORE COMPLETING FORM

1. REPORT NUMBER: AFOSR-TR-81-0184	2. GOVT ACCESSION NO.: AD-A095865
3. RECIPIENT'S CATALOG NUMBER	
4. TITLE (and Subtitle): Restrike Particle Beam Experiments on a Dense Plasma Focus.	5. TYPE OF REPORT & PERIOD COVERED: Interim, 30 Sept 1979 - 30 Sept 1980
	6. PERFORMING ORG. REPORT NUMBER
7. AUTHOR(s): GLENN GERDIN	8. CONTRACT OR GRANT NUMBER(s): AFOSR-79-0121
9. PERFORMING ORGANIZATION NAME AND ADDRESS: Fusion Studies Laboratory, 214 Nuclear Engineering Lab., Univ. of Illinois, Urbana, IL 61801	10. PROGRAM ELEMENT, PROJECT, TASK AREA & WORK UNIT NUMBERS: 61102F 2301/A7
11. CONTROLLING OFFICE NAME AND ADDRESS: Air Force Office of Scientific Research/NP, Building 410, Bolling AFB, DC 20332	12. REPORT DATE: Nov 1980
	13. NUMBER OF PAGES: 65
14. MONITORING AGENCY NAME & ADDRESS (if different from Controlling Office)	15. SECURITY CLASS. (of this report): Unclassified
	15a. DECLASSIFICATION DOWNGRADING SCHEDULE

16. DISTRIBUTION STATEMENT (of this Report)

Approved for public release; distribution unlimited

17. DISTRIBUTION STATEMENT (of the abstract entered in Block 20, if different from Report)

18. SUPPLEMENTARY NOTES

19. KEY WORDS (Continue on reverse side if necessary and identify by block number)

Dense Plasma Focus
Particle-Beam Diagnostics
Plasma Diagnostics
Dense Plasma Focus electron and ion beam energy spectra

20. ABSTRACT (Continue on reverse side if necessary and identify by block number)

Particle-beam diagnostic tools have been developed to study the particle beams generated by a dense plasma focus device (DPF). These tools include an ion Faraday cup, solid state nuclear track detectors (SSNTD), electron beam Rogowski coils, an electron beam Faraday cup, and an electron beam magnetic spectrometer. These tools (excepting the SSNTD) all have a bandwidth of greater than 100 MHz and experimental tests of these devices are consistent with theory. The SSNTD have been applied in a unique way to study deuteron

DD FORM 1 JAN 73 1473

Unclassified

SECURITY CLASSIFICATION OF THIS PAGE (When Data Entered)

AD A095865

DTIC FILE COPY

beams of high fluence (>10^{15}/cm^2) generated by the DPF and the preliminary results are consistent with the neutron yield of the DPF using a beam-target model for neutron generation. Electron and ion energy spectras of the accelerated electron and ion beams have been measured using the above tools and it is found that the number of particles per unit energy obey a power law with particle energy for both types of particles. The exponent of this power law is roughly the same for both types of particles and varies between -3.3 and -4.0. Parallel plate coupling between the DPF device and the capacitor bank and an 80 kV trigger pulse with a rise time of less than 5 ns on the mainbank spark gaps appear to result in superior DPF performance in terms of neutron yield when compared with other DPF devices of the same mainbank current or bank energy. The application of the results of this research to opening switch technology is discussed.

AFOSR-TR- 81-0184

RESTRIKE PARTICLE BEAM EXPERIMENTS ON A DENSE PLASMA FOCUS

Univ. of Illinois

AFOSR-79-0121

a) Annual Report Abstract

Particle-beam diagnostic tools have been developed to study the particle beams generated by a dense plasma focus device (DPF). These tools include an ion Faraday cup, solid state nuclear track detectors (SSNTD), electron beam Rogowski coils, an electron beam Faraday cup, and an electron beam magnetic spectrometer. These tools (excepting the SSNTD) all have a bandwidth of greater than 100 MHz and experimental tests of these devices are consistent with theory. The SSNTD have been applied in a unique way to study deuteron beams of high fluence ($10^{15}/cm^2$) generated by the CPF and the preliminary results are consistent with the neutron yield of the DPF using a beam-target model for neutron generation. Electron and ion energy spectra of the accelerated electron and ion beams have been measured using the above tools and it is found that the number of particles per unit energy obey a power law with particle energy for both types of particles. The exponent of this power law is roughly the same for both types of particles and varies between -3.3 and -4.0. Parallel plate coupling between the DPF device and the capacitor bank and an 80 kV trigger pulse with a rise time of less than 5 ns on the mainbank spark gaps appear to result in superior DPF performance in terms of neutron yield when compared with other DPF devices of the same mainbank current or bank energy. The application of the results of this research to opening switch technology is discussed.

b) Research Objectives

Several authors[1] have reported the observation of high energy particle beams generated by various plasma focus devices. Particle energies of equivalent to ten times the capacitor bank voltage (and more) were measured by X ray spectra[2] (electrons), witness plate studies[3] (electrons and ions), induced nuclear reactions[4] (ions), magnetic spectrometer (ions)[5] and time-of-flight (ions)[1,6]. Electron beam currents of up to 1.2 MA have been inferred from the X ray spectrum and thermoluminescent detectors.[7] Thus it would appear the dense plasma focus (D.P.F.) concept may play an important role in particle-beam technology.

The investigators supported by this contract, called 'Restrike Beam Experiments in a Dense Plasma Focus', have a general goal of devising and performing a series of experiments that will reveal the underlying physics of the acceleration mechanism. The specific and unique approach used is to adapt many of the diagnostic tools used in electron beam research to the environment of a dense plasma focus. These tools will be combined with more conventional dense plasma diagnostics (those of high temperature plasmas) to arrive at an empirical description of the scaling and nature of the acceleration phenomena. These data will be compared with numerical calculations designed to self-consistently simulate D.P.F. conditions during the acceleration process. In this manner it is felt that the possibilities of the D.P.F. as a collective particle accelerator can be fully appreciated.

In summary then the goals of the research ending on September 30, 1980 were as follows:

1) Develop particle beam diagnostics
   a) To determine how beam parameters scale with pressure and bank voltage.
   b) To use resultant data as a test comparison for predictions of a computer calculation.
2) Develop plasma diagnostics to determine conditions necessary for beam generation and as a further check on the computer calculations.
3) After analyzing present experimental results and surveying the literature begin to develop a theoretical model as the basis for a computer calculations.

The progress toward these objectives that was achieved is presented in the next section.

c) Status of the Research Effort

The main effort this year has been the design, construction, and testing of particle-beam diagnostics and significant results have been achieved. An ion beam Faraday cup has been designed, built and tested which is capable of measuring ion energy spectra in the 20 keV to 500 keV energy range[6] and solid state nuclear track detectors[8] have been employed in a unique way to get a measure of the total number of accelerated ions (deuterons). A fast, high-current Faraday cup to observe the electron primary current has been designed and built and is presently being tested as is a magnetic spectrometer to be used to measure the electron energy spectrum[9]. These accomplishments plus preliminary experimental results indicate that several interesting experiments should be possible in the next few months. Presently work is underway on developing a soft-X ray

spectrometer to measure some of the plasma conditions during the acceleration phase and on starting a parallel theoretical effort so the significance of the experimental results will be more fully understood. In the next four subsections the progress in beam diagnostics, plasma diagnostics, and D.P.F. operation, respectively, will be summarized. At present the theoretical effort is too preliminary to be included in this report. Finally the application of this research to opening switch technology is discussed.

Particle-Beam Measurements

As discussed in section b, several investigators have reported measurements of the effects of particle beams generated by plasma foci. The research effort described here has been directed toward measuring the parameters of the beams as directly as possible such as measuring currents produced by beam particles directly such as in Faraday cup collection rather than more indirect methods such as unfolding the electron energy spectra from the hard X ray spectra.[2] While these methods are commonly used in electron beam research the difference in the working pressure between a D.P.F. and an electron-beam diode make the adaption of these techniques of electron-beam research to D.P.F. research non-trivial. The higher working pressures of a D.P.F. ($p \sim 1$ torr) can cause severe attenuation of the lower part of the ion energy spectrum and plasma currents produced by these beams in passing through this gas can make the interpretation of the results difficult. This year success has been achieved in eliminating these problems and accordingly a combination of electron-beam type diagnostic tools is now available for our D.P.F. experiments. Thus the results of these experiments should be complementary to previous studies and unique in their own right. In the following paragraphs, the ion-Faraday cup, the

SSNTD results, the electron Faraday cup, the electron magnetic spectrometer and preliminary scaling experiments will be discussed.

Ion Faraday Cup

Although several[10] dense plasma focus (DPF) experiments exist, the mechanism for neutron production (when deuterium is used as a fill gas) has yet to be described in a satisfactory manner. The anisotropy[10,11] of the neutron yield from such devices suggests that beam-target neutron generation may be important, which indicates a need for determining the energy spectrum of accelerated ions.

Other investigators have used activation analysis of nuclear reactions produced by fast deuterons,[4,12] a magnetic spectrometer,[5,13] and time of flight using PIN diode detectors [1,14] to determine a portion of the energy spectrum of deuterons emitted by the focus. In order to record the energy spectrum, the magnetic spectrometer used scintillation and photographic film which is somewhat cumbersome. The lack of differential pumping in all these cases limits the energies resolved to above 100 keV.

In the experiments reported here, a tube with a 0.0457 cm diameter hole at one end was inserted along the axis of a Mather-type DPF to a point 16 cm from the top of the anode (Figure 1). Thus most of the flight path of the ions from the focus to the cup is at a pressure of 10-20 which significantly reduces the attenuation of the ion energy as compared with previously reported investigations.[1,4,5,12-14] A plastic scintillator-photomultiplier combination was used to observe the start of the hard X-rays produced by electron-target interaction to determine the time of acceleration for time-of-flight analysis. Such a combination of diagnostic

tools to measure the ion energy spectrum has several advantages over the other methods in that it is simple, cheap, rugged, convenient and can resolve the ion energy spectrum by time of flight to significantly lower energies. The lower energy deuterons may play a significant role[10,11] in neutron production, so this is an important advance.

The passage of the beam through the gas between the focus and the hole (and to a lesser extent the passage through the differentially pumped region) has three major influences on the beam properties. These are

1) The neutral gas removes energy from the beam particles.[15]
2) The neutral gas broadens the beam through multiple scattering.[16]
3) The beam particles capture and lose electrons to the gas to form an equilibrium charge state.[17]

All these effects are more severe at lower beam energies and hence tend to reduce the signal-to-noise ratio in such a way as to estblish an effective lower energy cut-off. The first two effects can be greatly reduced using the differentially pumped drift tube as shown in Figure 1. However, even the 10μ of gas pressure in the drift space is sufficient to establish an equilibrium charge state.[17,18] Since the equilibrium ionic fraction falls below 10% at about 12 keV for protons in hydrogen (or ~24 keV for deuterons), these energies probably represent an effective lower limit to the energy resolution of this detector. Removing the 500 G magnetic field from the cup (the field is used in the magnetic ion collector mode or MIC mode) and operating the cup to observe secondary electron emission (SEE mode) would make the cup sensitive to neutrals as well. However, the secondary emission coefficient falls off rapidly[19] with decreasing particle energy in the 0 to 50 keV region so the effective lower energy limit for the SEE mode of operation is about the same.

Thus the overall features of the differentially pumped drift tube concept are five-fold:

1) Lower energy attenuation of the beam by neutral gas
2) Lower lateral spread of the beam caused by multiple scattering
3) Minimal effect of the hole potential because of plasma formed by the beam
4) Long beam-drift region at 10-20μ pressure which sets an equilibrium charge state independent of conditions in the DPF chamber
5) Lower correctable energy limit extended to about 25 keV.

To determine the start of the acceleration process it was decided to use the hard X-ray spike measured with a plastic scintillator (Pilot B) and a fast rise time photomultiplier tube (Amperex XP2230). As will be seen below, the acceleration process appears to be that of a plasma diode and hence electrons get accelerated at the same instant as the ions and run into the anode and lower portions of the device generating hard X-rays in a time period short with respect to the ion flight time to the cup.

Using this combination of diagnostic tools, the performance of the Faraday cup was evaluated. Typical signals for shots taken for the cup operated in the MIC mode and the grid (Figure 2) in the SEE mode are shown in Figure 3(b) and 3(c) respectively. The grid signal is similar to that of the cup in the SEE mode. The signal is believed to be ions on the basis of the following:

1) The Faraday cup was found to have a plateau response between -200 V and -450 volts.
2) Only positive signals were obtained.
3) When using D_2, no ion current was detected when the neutron yield was negligible.

4) The ion signal always arrives after the current singularity and the X-ray spike occur.

5) For an anode-cup distance of 94 cm two peaks were observed when equal mixtures of hydrogen and deuterium were used (Figure 4) and the cup was operated as a secondary emitter.

6) The two modes of operation, as a secondary electron emitter (SEE mode) and as an ion collector (MIC model), were found to give consistent results.

Perhaps the most convincing evidence of the observation of ions on the Faraday cup is the observation of two peaks when mixtures of hydrogen and deuterium are used in the static filling of the main DPF chamber. It was found that the cup has to be operated in the SEE mode to increase the signal strength and that the anode-cup distance had to be increased to 94 cm from 48 cm to adequately resolve the two signal peaks. The appearance of two peaks (Figure 4) represents plasma-diode (constant potential) acceleration away from the anode and has been reported previously by Gullickson et al.[1] using PIN diode detectors for the fast ions. Using the initiating time as the rise of the X-ray pulse on the SPMT, the ratio of the time to the second peak (assuming it represents D) to that of the first peak (assuming it is H) should be $\sqrt{2}$. This ratio is plotted versus mean deuteron energy for a series of shots in Figure 5. As can be seen the data will cluster about the theoretical value of $\sqrt{2}$.

This plasma-diode action is consistent with earlier observations[21-24] of the net electron current traveling through the hollow anode of the DPF in the opposite direction from the deuterons occuring during the emission of hard X-rays.

The design feature which makes this charge collector system unique is that the major portion of the flight path is at relatively low gas pressure through the use of a differentially pumped drift tube. The path makes it possible to observe ion energies to considerably lower values than is possible when such a drift tube is not used. Finally, the attenuation effect of the focus plasma itself was analyzed and found to be small for a typical focus plasma, e.g. $n \sim 10^{19}/cm$ and $T_e \sim 1$ keV.

The data of five shots each give an ion energy spectra of the general shape

$$\frac{dN}{dE} = CE^{-3.5}, \text{ for } 25 \text{ keV} \leq E \leq 500 \text{ keV}$$

where the Faraday cup was used in MIC mode and corrections for charge state, lateral spread and energy attenuation by the working gas have been made. Two of the spectra involve small bumps-on-the-tail, but on both sides the energy spectrum displays the $E^{-3.5}$ dependence. These data shows much more uniformity than that of other investigators[25] and may be due to the lower energy capability of this diagnostic tool. It also represents a useful check on any theoretical model of ion acceleration.

Solid State Nuclear Track Detectors (SSNTD)

The desire to measure quantitatively the number of deuterons accelerated above same energy and the chance visit by R. Ilic', an expert on SSNTD, from the J. Stefan Institute, Ljubjana, Yugoslavia, motivated the interest in using SSNTD for deuteron observation. The principle of SSTND is as follows: heavy charged particles create damage sights in the detector (usually plastic) and after etching the detector in a caustic solution, the damage sights become pits or holes which can be observed under an optical microscope and counted. The SSTND have these advantages over other techniques (such as nuclear emulsions):

1) SSNTD are insensitive to light, electrons or Xrays
2) Record is virtually permanent
3) Direct measurement of fast particles is possible and (detection efficiency can be made to be one)

However the maximum track density that can be counted is less than $10^7 cm^{-2}$. Since the total number of deuterons accelerated in a DPF may be greater than $10^{15}/cm^2$, fluences much greater than the SSNTD track density limit may easily be encountered. Thus if some quantitative means of reducing the detection efficiency for deuterons could be found these detectors could become quite useful for the observation of deuteron beams generated by a D.P.F.

If the detector were covered by a layer of material which contained an isotope that has a low energy threshold nuclear cross section for (d,α) reactions and only alphas are detected by the SSNTD the effective deuteron detection efficiency can be greatly reduced. A survey of the existing SSNTD revealed a type known as 'LR115 type IIB stripping' which has an

108 μm layer of $Li_2B_4O_7$ on a 15 μm layer of cellulose nitrate on a 100 μm thick polyesther backing. The ^6Li and ^{10}B in the $Li_2B_4O_7$ layer have significant (d,α) cross section and produce alphas energetic enough to penetrate the $Li_2B_4O_7$ layer after being generated on its surface and create tracks in the cellulose nitrate SSNTD. The low energy threshold for $^6Li(d,\alpha)^4He$ and $^{10}B(d,\alpha)^8Be$ are roughly 150 keV and 1 MeV respectively. Thus for a 150 keV deuteron beam the track creation efficiency as estimated by a thick target calculation[26] for $^6Li(d,\alpha)^4He$ is 10^{-11} track/deuteron. Hence if the deuteron fluences are 10^{14}-$10^{15}/cm^2$ per shot in the DPF the track densities would be $\sim 10^3$-$10^4/cm^2$ which is almost the ideal density for SSNTD track counting. Thus the LR115 type IIB SSNTD would appear to be most suited for quantitative deuteron beam measurements in a DPF for the following reasons:

1) LR115 is relatively insensitive to singly charged ions (i.e., p, d, t)
2) $^6Li(d,\alpha)^4He$ produces alphas energetic enough to pass through the $Li_2B_4O_7$ layer
3) Deuterons have to have energies of greater than 2.2 MeV to penetrate the $Li_2B_4O_7$ layer (1.65 MeV for protons).

To test the feasibility of the converter layer concept two experiments were performed. One using a deuteron beam of known properties produced in a neutron generator to compare the measured track production efficiency with thick target yield calculations.[26] A 150 keV beam was used which is too low an energy to penetrate the $Li_2B_4O_7$ layer or to produce $^{10}B(d,\alpha)^8Be$ reactions. The second experiment involved the simultaneous irradiation of

LRN5 type II (with the $Li_2B_4O_7$ converter layer) and LR115 with the $Li_2B_4O_7$ replaced a sheet of mylar with thickness such that it is equivalent to the $Li_2B_4O_7$ in stopping power. In the mylar no (d,α) reactions can occur, but the fast deuterons that penetrate both $Li_2B_4O_7$ and the mylar should have the same effect on the SSNTD in each case.

Thus the effect of fast primary deuterons may be separated from that of the secondary (d,α) alphas so that a quantitative measurement can be made even when the fast deuteron (E_D > 2.2 MeV) component is present. Since deuterons of energies even greater than 5 MeV have been reported to be generated by DPF, the effect of these deuterons on the SSNTD could be cause for conccern.

The SLR115 type II detector was irradiated in a Texas Nuclear neutron generator by a 5-6 μA beam of 150 keV deuterons (figure 6). The polyester backing was removed to improve the thermal contact between the cellulose nitrate (CN) layer and the water cooled back plate of the neutron generator. A copper plate with 0.36 mm diameter holes was placed over the lithium tetraborate layer to further reduce the heating of the detector and to measure the beam current.

A typical picture taken from a view of CN surrounding an irradiated hole is shown in Figure 7. Note the roughly circular pattern of the etched alpha tracks indicating the position of the hole. The mean track density was calculated by summing up all the tracks in all the holes and dividing by the total hole area. This density was then divided by the mean beam fluence to determine the measured efficiency in track production per incident deuteron.

The results of two such calibrations are compared in Table I with the thick target alpha track yield calculation using known $^{6}Li(d,\alpha)^{4}He$ cross sections[28] and stopping power in $Li_2B_4O_7$[15]. The allowable solid angle was determined from the range of 11.2 MeV alphas in $Li_2B_4O_7$.

Table I

	Track product efficiency for 150 keV deuterons
neutron generator irrad. I	$3.05 \cdot 10^{-11}$ track/deuteron
" " " II	$4.17 \cdot 10^{-11}$ track/deuteron
thick target track yield calc.	$1.17 \cdot 10^{-11}$ track/deuteron

While there is some discrepancy between the thick target calculation and the irradiations, the consistency between irradiations is good enough to make this technique look promising. Cross section uncertainties for $^{6}Li(d,\alpha)^{4}He$ and possible detection of $^{6}Li(d,p)^{7}Li$ protons may explain some of the discrepancy. The latter possibility appears to be in conflict with the results of the DPF irradiations and Kodak France specification[27] for LR115 which indicate LR115 is sensitive only to protons of energy less than 100 keV.

The irradiation of LR115 type II and LR115 with a mylar cover were carried out in the DPF in the configuration shown in figure 8. Here again the polyester backing of the two types of LR115 was removed to improve thermal contact with a heat sink and a copper plate with 1 mm holes was placed over the various cover layers to further reduce heating of the CN. It was determined that 100 μm of $Li_2B_4O_7$ was equivalent to about $\simeq$ 1.6 mil of mylar (figure 9) so cover thickness of B (figure 8) and that of C were made 1.5 mil and 2.0 mylar respectively. Typical holes exposed to the DPF

and an unirradiated LR115 type II detector are shown in figures 10-13. In figure 10 representing the irradiated LR115 type II, both large tracks and small tracks are present in the hole area. Since the larger tracks correspond in size to those seen in the neutron generator irradiation where only alphas should have been observable, these tracks are identified as those produced by alphas from the (d,α) reactions in $Li_2B_4O_7$. The smaller pits are assumed to be caused by deuterons in the tail of the ion distribution caused by DPF acceleration. That this explanation is feasible is shown in figure 11, the LR115 covered by 1.5 mils of mylar. Here numerous small pits are observed with densities comparable to that of the small holes in figure 10 indicating that portion of the tail of the ion energy spectrum that just makes it through the mylar with $\leq$ 100 keV of energy to spare create the pits. 3.0 MeV protons produced by D(d,p)T reaction in the focus should be able to penetrate 2 mil of mylar with $\gtrsim$ 1.0 MeV remaining and create tracks with densities comparable to the $^{6}Li(D,\alpha)^{4}He$ alphas for the configuration shown in figure 8. The fact that no tracks are observable in figure 12 indicates that the sensitivity of LR115 must be extremely low to high energy protons and that the deuterium energy distribution effectively falls to zero below 2.3 MeV (figure 9). The background hole density is shown in figure 13 and indicate that the hole density in figure 10 is significantly above background (probably α from radon gas).

Thus the problem of detecting energetic deuterons by LR115 appears manageable on the basis of difference in hole size and detection effeciency.

Using the ion energy spectrum observed on the Faraday cup by time of flight and assuming the energy spectrum is the same in all directions subtended by the target plate (figure 8) one can estimate the total number

of deuterons accelerated and hence determine a target thickness for neutron production from the neutron yield. The results of these crude assumptions are as follows

Table II

Quantity	
Target thickness $n_T \ell_T$	$1.6 \cdot 10^{19} cm^{-2}$
Number of deuterons accelerated above 100 keV	$N_D(>100 \text{ keV}) = 3.10^{15}$
Total Deuteron Energy (> 100 keV)	80J
Efficiency of fast deuteron production	$6 \cdot 10^{-3}$

The fact that none of these numbers is unreasonable for a DPF indicates the plausibility of the results and the promise of further experimental results using this technique.

Electron Current Rogowski Coil

Among the earliest diagnostics[21-24] to be implemented to study the fast particles generated by a plasma focus, the Rogowski coil[29] is a toroidal magnetic pickup coil used to measure currents passing through the major midplane of the coil. Because counter-currents are generated in the plasma produced by the electron beam plasma interaction at DPF pressures, the usefulness of this diagnostic is somewhat limited. Nevertheless, we have performed several scaling experiments and have observed some very encouraging data on the scaling of the Rogowski current (or net electron current, I_{net}) with the main bank current at pinch time.

In a series of experiments at 25 kV in deuterium gas at varying pressures performed between January and November 1979 correlations between neutron yield and net electron current passing through the center anode were observed such as that shown in Figure 14. This indicated a simple beam-target model might be used to explain the neutron yield in the devide[22,23] and this tended to be confirmed by the strong anisotropy of neutron flux as recorded on the forward and side silver activation detectors.

These results were interesting since net electron currents of up to ~11 kA were observed and peak electron energies greater than 100 keV could be inferred from Hard X rays signals (figure 15).

However, at the static pressure used in DPF experiments, the net current is lower limit to the electron beam current and the hard X ray filter only gives alower limit to the beam's energy since it observes X rays above 100 keV. The net electron current is a lower limit to the beam current because $\dot{B}$ forces in the head[30] of the beam can produce return currents in the plasma formed by the passage of the beam. This effect is especially pronounced

in the range[30] of ambient pressure around 1 torr which is also the range of most efficient electron energy transport and is the range of pressure of DPF operation. It is also found that beams propagate over distances of interest if $I_{net} = |\vec{I}\ \text{primary} + \vec{I}\ \text{plasma}| \leq 17000\beta\gamma(\text{Amperes})$. Since the largest net current we have measured[23] is 11.3 kA we may be close to the net current limit (if the mean electron energy were 103 keV then $\beta\gamma = 2/3$).

That plasma current effects dominate the e beam transport can be seen by the slow decay of the net Rogowski signal as opposed to the period of duration of the hard X ray spike (figure 15). Subsequent experiments indicate the duration, τ, of the primary electron current is that of the hard X rays or less than 50 nanoseconds. As seen in figure 15, the net current displays almost exponential decay with an e folding period of about 200 nanoseconds. Assuming the electron beam's magnetic field is trapped in the plasma formed when the gas breaks down, the decay time will be the magnetic diffusion time for a plasma of the inner radius of the anode. Assuming this plasma is fully ionized and classical Spitzer resistivity,[31] this decay time corresponds to a plasma electron temperature of about 1.7 eV. Clearly a resonable value for this situation.

After a broken insulator had been replaced and after a period of several days when conditioning discharges had been made, the experiments to measure the scaling of the net electron current with bank parameters were performed. The results are shown in figure 16 for a range of voltages in with different filling pressures of hydrogen as a parameter.

As can be seen, at a given pressure the net electron current increases with voltage until a certain voltage is reached when a fall off in net current occurs. If the run in time is plotted as a function of voltage (figure 17) it is seen that the net electron current stops increasing when the run in

time deviates from the snow plow model and shows some evidence that a minimum has been reached. Since the voltage across the electrodes, V_{io}, for a varying inductance $\dot{L}$, due to the moving current, I, is given by

$$V_{io} \sim I\dot{L} \sim I \frac{\mu_o}{2\pi} \ln \frac{R_o}{R_i} v_s$$

where R_o is the outer electrode radius, R_i is the anode radius and v_s is the velocity of the current sheath. From the snow plow model

$$v_s \sim \frac{l}{t_R} \sim \frac{V^{1/2}}{p_o^{1/4}} \text{ and } I \sim V$$

where l is the length of the exposed anode, t_R is the run in time', V is the bank voltage and p_o is the filling pressure. When V_{io} is equal to the breakdown voltage between the electrodes parasitic currents can form and rob the current sheath of its force. This should occur at increasing bank voltages as the fill pressure is increased when

$$p_o^{1/4} \sim V^{3/2}$$

or

$$p_o \sim V^6$$

The experimental results from figure 16 are shown in figure 18. Using least square analysis, the fill pressure was found to scale as the bank voltage (where the net electron current falls off) to the power 5.2 ± 1.2. As seen in the figure a slope of six fits the 2-4 torr data very well. This is strong indication that parasitic currents are forming and spoiling scaling for the data to the right of the arrows in figure 16, and therefore these data should not be used in scaling. That is they represent performance when the DPF is not operating properly and this type of performance can be eliminated by more electrode conditioning (if the insulator is gassy), by inserting an outer electrode with smoother edges, or by reducing R_o/R_i (by increasing R_i and keeping R_o-R_i constant).

In an experiment at 3 torr in hydrogen simultaneous pictures of mainbank current and net electron current were taken. The data taken below the breakover voltage for 3 torr in hydrogen (figure 16) are plotted in figure 19. The net electron current is found to increase with mainbank current to the power 3.3 ± 0.6. More experiments are planned to try to reduce the error and measure the effect of different gases.

The steep dependence on I_{net} on the mainbank current could clarify the nature of the data in figure 14.

A question arises from this data and that is why does the addition of impurities lower the net electron current (figure 14)? One effect of the addition of N_2 into the filling gas is that the additional mass slows down the current sheath and causes it to collapse when the mainbank current is lower (the pinch in our device arrives after the maximum in the mainbank current). Since the net electron current scales so steeply with mainbank current it is possible that this effect alone could be the answer to the question. Using the snow plow model and mainbank current data at 2 torr with no impurities (we will do some confirming experiments later) and the comparing the highest neutron yield shots (where the snow plow model should hold) the data are summarized in Table 1.

Table 1

Shot	Neutron Yield	Deuterium partial pressure (torr)	Nitrogen partial pressure (microns)	I_{MB} relative units	pre-dicted I_{net}	measured I_{net}
7/9/79 #5	$2.49 \cdot 10^9$	2.0	0	0.94	11.5 kA	11.5 kA
5/28/79 #40	$1.94 \cdot 10^9$	2.0	50μ	0.876	9.2 kA	9.8 kA
5/28/79 #16	$4.5 \cdot 10^8$	2.0	200μ	0.689	4.0 kA	5.5 kA
5/29/79 #1	$2.87 \cdot 10^9$	1.5	0	0.977	16.8 kA	16.8 kA
5/29/79 #11	$2.46 \cdot 10^9$	1.5	50μ	0.926	14.0 kA	12 kA
5/28/79 #30	$3.9 \cdot 10^8$	1.5	200μ	0.729	6.4 kA	8 kA

The predictions have been normalized to the I_{net} current with no nitrogen added at each pressure of D_2. It can be seen that the slowing of current sheath by the additional mass can indeed account for the lowering of I_{net}. This gives added confidence in the measured scaling shown in figure 19 and helps one understand earlier results.

Electron Beam Faraday Cup

A high current, nanosecond rise time Faraday cup has been constructed to measure the primary current of the DPF generated electron beam. A thin (5 mil) Mylar foil is placed across the evacuated Faraday cup to prevent the formation of a return current inside the cup. The mylar is thin enough to permit the passage of high energy ($\geq$ 120 keV) electrons but prevents the flow of any induced plasma current that might form inside the evacuated region ($\simeq$ 50 μm) of the cup. The mylar foil is placed within 2 mm of the cup electrode to minimize beam blow up.

The Faraday cup design is based on the cup built by Pellinen[32] as shown in Figure 20a). In order to derive design criteria for the Faraday cup the high frequency response of the cup is calculated for a step function current input. In order to insure that the cup output is linear up to a frequency w, it is found[33] necessary to have

(1) $R_s \ll \sqrt{\frac{L}{C}}$

(2) $\frac{L}{R_s} \ll \frac{2\pi}{w}$ or $\frac{1}{\sqrt{LC}} \gg w$

where L and C are the inductance and capacitance of the cup, and R_s is the resistance of the stainless steel shunt. The peak voltage across the cup reaches $I\sqrt{\frac{L}{C}}$, so it is also required to have

(3) $I\sqrt{\frac{L}{C}} \ll$ mylar transient breakdown voltage where I is the input current.

Aluminum is used for the center electrode instead of carbon since carbon has a non-negligible skin depth for frequencies of interest. The inductance of 3×10^{-11} H quoted in reference 32 is inaccurate because the finite skin depth of carbon is neglected; at 100 MHz, the inductance is actually more than twice this value. Since aluminum has a much higher conductivity than carbon, a Faraday cup made with aluminum will typically have a much lower inductance. The stainless steel shunt is made thin compared to a skin depth to insure that the resistance of the shunt is independent of frequency, but it is also made thick enough so that output voltages are observable directly with an oscilloscope.

The estimated bandwidth of the Faraday cup[33] is 200 MHz. It has been calibrated with a 20 kA capacitor discharge and is found to have a 3.4 mΩ resistance (calculated value = 3.5 mΩ). The cup response to the primary current of the DPF electron beam is shown in Figure 20b). The short time duration of the primary electron beam is consistent with the hard x-ray signal (Figure 15b) and in sharp contrast to the net electron current signal (Figure 15a). This diagnostic appears to be performing as desired.

Electron Magnetic Spectrometer

A magnetic spectrometer has been constructed to determine the energy spectrum of the DPF generated electron beam (Figure 21). Some of spectrometer characteristics are listed as follows:

(1) The 3 torr DPF fill gas is used for beam transport since it lies within the optimum pressure range for beam transport in deuterium.

(2) Aluminum is used in the construction of the drift tube and spectrometer to minimize scattering and hard x-ray production.

(3) Collimators limit the collected current to a few milliamps to prevent collective effects[34] from disrupting beam electron orbits.

(4) An Armco fringe field shield reduces the fringe field in the collimating region by $\sim 10^{-3}$.

(5) 11 Faraday cup collectors are available to cover an energy range of ~10 keV to ~10 MeV when B ≈ 200 Gauss.

(6) The Faraday cups are situated in the fringe field of the electromagnet to inhibit secondary electron emission.

(7) Since Faraday cups are used, time resolved spectra can be obtained (the system rise time is determined by the oscilloscope bandwidth (100 MHz)).

(8) Time integrated spectra can also be obtained by using the signal cable capacitance and a high impedance termination, such as the typical oscilloscope input (e.e. 1 mΩ).

(9) The error in the energy measurements is due mainly to the finite width of the collimators and is estimated to be ~10%.

Preliminary results have been obtained with the spectrometer at 3 torr D_2. Figure 22 shows time resolved signals for two channels. Figure 22(a), the lower energy channel, displays two main peaks which occur before and after the single higher energy peak in Figure 22(b). This is indicative of the rise and fall of the accelerating potential and is similar to data obtained with e-beam diodes.[35] The time resolution is limited by the oscilloscope bandwidth. Time integrated spectra have been obtained with four channels and are shown in Figure 23. All of the spectra are similar and seem to follow a power law:

$$\left.\frac{dN}{dE}\right|_{\text{eletrons}} \propto E^{-a} \quad 3.3 < a < 4.0 \ .$$

Simultaneous electron and ion energy spectra have also been obtained and are essentially identical (see Figure 24), which suggests a plasma diode accelerating mechanism.

The magnetic spectrometer will be used together with the high current Faraday cup to determine the voltage, current and perverance characteristics of the DPF acceleration process. Results will be used to compare the DPF "diode" with standard diode models and with a 1-D hydrodynamic code.

Plasma Diagnostic: Soft X-ray Spectrometer

Since the electron thermal speed is important in assessing the likelihood of various microinstabilities causing anomalous resistivity[36] and since the knowing electron temperature as a function of time would be an important check on the results of any magnetohydrodynamic model for the focus,[37] it was decided to develop a soft x-ray spectrometer using pin diodes and Ross filters.

A hot plasma emits X-ray radiation due to 3 main processes.

1. Bremsstrahlung from free-free transitions in the plasma.
2. Recombination from free-bound transitions in the plasma.
3. Line radiation from bound-bound transitions in ahd plasma and in the impurities present.

The first two types of radiation follow an exponential dependence on the temperature, while the third type also depends heavily on the amount of impurities present in the plasma.

If the third component (line radiation) can be isolated and taken out of the spectrum, then it is possible to determine the temperature of the plasma by analyzing the residual radiation emission.

The line component can be filtered out by the use of Ross balanced filters. The soft X-ray spectrometer, a part of the diagnostics for the Dense Plasma Focus experiment, was designed to measure the temperature of the plasma. The principle of operation of the spectrometer is the detection and analysis

of selected frequency bands of the X-ray spectrum using filtered PIN-DIODE detectors.

The bands are delimited by Ross balanced filtering technique. This technique uses the fact that the stopping power for xrays has sharp edges at different frequencies for different materials. Using foils that have the same stopping power at all but a certain frequency band, it is possible, by taking the difference of the signals, to reconstruct the energy emitted by the plasma in the given frequency band. This fact enables one to select regions of the spectrum which are free from line radiation. The this is feasible in our Dense Plasma Focus, because the only component that must be filtered out is the Cu k-line radiation, which is concentrated in the 8keV region.

The use of PIN-diodes detectors enables one to scan the region between 1 and 8 keV, thus making it possible to estimate the temperature of the focus.

There are three PIN diode detectors in the spectrometer, which make up two channels, with proper filters. The signal from each PIN diode gives a time resolved picture of the x-ray emission. The amplitudes from the detectors of a channel are subtracted from one another to find out the energy released in each channel. The ratio of the intensities of each channel depends on the temperature of the plasma, and it is fed into a computer program which then gives out an estimate value of the temperature in the plasma.

Physically the Xray spectrometer is a muffler shaped aluminum tube, made up of 5 section (Figure 25).

1. Detectors holder

Shielded with lead sheets. The three detectors are located at the end of the tube with a 120° circular symmetry. The filters (metal foils) are held in front of the PIN-diodes by expecially machined holders at certain

angles, to achieve the desired stopping power. A combination of Al, Fe, Ni, Ti foils has been provided.

2. Collimation section

Shielded with lead sheets. It has two horizontally slotted tantalum collimators.

3. Insulating section

Made of plexiglass. It prevents the rise in potential occurring in the focus from reaching the detection system. This part has to provide a long enough non-conductive space so that discharge across it cannot occur in operating conditions.

4. Vacuum pump connection

The whole path of flight of the X-rays has to be under vacuum. The vacuum is provided by a two stage mechanical pump, which is able to reach ~1 micron of pressure.

5. Bellows and Adaptor Flange

The bellows allow a certain freedom of movement to the spectrometer and frees the dense plasma focus from mechanical stresses. Through the use of the bellows it is possible to aim the spectrometer at different points in the focus. The flange is the connecting link between the D.P.F., and the spectrometer chambers. The flange holds the beryllum foil which is needed to close the bacuum in the spectrometer.

Some preliminary results using the soft Xray spectrometer in a single channel mode are that strong signals are observed at pinch time through a 10 mil beryllium window and that no signal is observed when the beryllium window is replaced with an 1/8" thick aluminum plate. These results are encouraging because they indicate that good signal to noise ratios may be expected and the effects of hard Xrays and electromagnetic noise have been minimized. It is expected that the spectrometer will become fully operational in the next few months.

General Operation of the D.P.F. Device

Classic operation[38] of the Illinois D.P.F. is evidenced by the measured dependence of the run-in time on bank voltage and filling pressure (figure 26) and by the fourth power law of the main bank current at pinch time (figure 27). In fact, the neutron yield is significantly higher than those reported[10] in the literature for foci of the same bank energy and main bank current. The calibration of our silver activation yield detector of neutron using neutrons from $D(d,n)^3He$ produced in a neutron generator (figure 6) gives strong support to this contension. Also the experimental tests of the main bank Rogowski coil by capacitive discharge were found to be self consistent with theoretical calculations.

The excellent performance of the Illinois D.P.F. is believed to be caused by two design features:

1) Parallel plate connections between the device and the four capacitor banks;
2) A fast rise time high voltage pulse that triggers all four main bank spark gaps.

The first feature enables more efficient use of magnetic energy in the field contributing to the pinch rather than being merely stored in other places such as coupling cables (i.e. lowers the external inductance). The second feature insures that the magnetic energy is delivered in a symmetric fashion. A two stage Marx generator has been designed, built and operated[39] that delivers 80 kV pulse with a rise time of less than five nanoseconds to each of the four trigger pins of the main bank spark gaps which are set for self breakdown at just above the operating of voltage of the bank (usually 25 kV). Using magnetic pickup loops the jitter of the mainbank spark gaps

has been measured to be less than 20 ns. The effect of the low spark gap jitter is revealed in the main bank current waveform as measured on the main bank Rogowski belt (figure 28). The sharp indentation of the current waveform at pinch time and the low amplitude of the current oscillations in the post pinch phase indicates a large fraction of magnetic energy is coupled to the D.P.F. plasma and particle beams. Thus the performance of the Illinois device has been extremely good.

The Relation of the Research to Opening Switch Technology

The development of the beam and plasma diagnostics for the dense plasma focus and the apparent generation of particle beams by current interruption, suggest that a near term application of this work could be the study of the physics of a high pressure opening switch. As seen in Figure 28, the total current in the Illinois DPF drops abruptly at pinch time with an instaneous time rate of change of current of $\sim 2 \cdot 10^{12}$ Amps/sec. This value is within an order of magnitude of the state-of-the-art opening switch experiments[40] and only 12 kJ of energy is involved. Although the DPF itself may not prove to be the eventual choice as an opening switch, it does make an excellent test bed for the development of diagnostics and theoretical models that can be applied to the plasma opening switch concept as well. Once these research tools are developed they can be applied to other types of opening switches such as exploding foils and wires where the set-up time is considerably longer.

Recent development of a 1MW N_2 laser by the Illinois DPF group will make it possible to obtain time and spatially resolved plasma density profiles by interferometric techniques.[41] This advance plus the soft Xray spectrometer should enable the formation of a fairly complete picture of the plasma phenomena as well as that of the beams for input into the theoretical

modeling already underway. Thus besides studying the physics of the DPF as a particle accelerator, the Illinois DPF research is also being applied to a limiting pulsed power technology[42], that of the opening switch.

d) Cumulative Chronological List of Publications

G. Gerdin, W.A. Stygar, F. Venneri, "Faraday Cup Analysis of Ion Beams Produced by a Dense Plasma Focus," accepted for publication in *J. of Applied Phys.*

In preparation

W. Stygar and G. Gerdin, "Rogowski coil rise time calculations for arbitrary terminating impedeance" to be submitted to J. of Plasma Physics.

R. Ilić, G. Gerdin and J. Durham, "Detection of High Fluence Light Ion Beams Using Solid State Nuclear Tract Detectors" to be submitted to Solid State Nuclear Tract Detectors (Pergamon Press).

W. Stygar, G. Gerdin and F. Venneri, "Simultaneous Measurements of the Energy Spectra of Ion and Electron Beams Generated by a Dense Plasma Focus" to be submitted to Phys. Fluids or Nuclear Fusion.

e) List of Professional Personnel Associated with the Research Effort

Personnel

Glenn Gerdin, Asst. Professor Nuclear Engineering, Principal Investigator

William Stygar, graduate assistant supported by AFOSR

Francesco Venneri, graduate assistant supported by AFOSR (started Jan. 1980)

James Durham, graduate assistant supported by University of Illinois Research Board (started June 1980)

James Mandrekas, graduate assistant supported by seed money of Univ. of Illinois Nuclear Engineering Program

Advanced Degrees

Jan. 1980, William Stygar, Master of Science in Nuclear Engineering, University of Illinois at Urbana-Champaign, thesis title "Design, Construction, and Operation of a Fast Rise Time, High Voltage Pulse Generator."

f) Interactions

Conference Papers

Fall 1979 meeting of the Plasma Physics Div. of the American Physical Society.

W. Stygar and G. Gerdin, Bull. Amer. Phys. Soc. 24, 1039 (1979).

Spring 1980 IEEE Conf. on Plasma Science at Madison Wisconsin.

G. Gerdin, W. Stygar and F. Venneri, Conf. Record--Abstracts 1980 IEEE Int. Conf. on Plasma Sci., IEEE 80CHI544-6, 75 (1980).

Fall 1980 meeting of the Plasma Phys. Div. of the American Physical Soc.

R. Ilić, G. Gerdin, J. Durham, B. Wehring, W. Stygar, T. Emoto, Bull. Amer. Phys. Soc. 25, 962 (1980).

W. A. Stygar, G. Gerdin, F. Venneri, Ibid 833.

Seminars

U. of I. Nuclear Engineering Program Seminar, Dec. 2, 1980.

1. R. L. Gullickson, J. W. McClure, W. L. Pickles, D. F. Price, T. E. Wainwright and M. D. Williams, 1980 IEEE Inter. Conf. on Plasma Sci. Conf. Rec. Abstracts, IEEE Catalog No. 80CH1544-6 NPS, p. 75 (1980).

2. J. H. Lee, et.al, Plasma Physics, 13, 347 (1971).

3. V. Nardi, W. H. Bostick, J. Feugas, W. Prior, C. Cortese, Plasma Phys. and Contr. Nucl. Fus. Research 1978 (Proc. 7th Int. Conf. 1978) 3, IAEA, Vienna (1979), 143. G. M. Molen, Aerospace Corp. Rep. (8 April 1976).

4. R. L. Gullickson and H. L. Sahlin, J. Appl. Phys. 49, 1099 (1978).

5. H. Krompholz, L. Michel, K. H. Schonbach, and Heinz Fischer, Appl. Phys. 13, 29 (1977).

6. G. Gerdin, W. Stygar and F. Venneri, Fusion Studies Lab Report FSL-16, Univ. of Illinois, Urbana, IL. 61801 (1980).

7. R. L. Gullickson and R. H. Bartlett, Advances in X ray Analysis, 18, p. 184 (1971).

8. R. Ilic, G. Gerdin, J. Durham, B. Wehring, W. Stygar, T. Emoto, Bull. Amer. Phys. Soc. 25, 962 (1980).

9. W. A. Stygar, G. Gerdin, F. Venneri, Bull. Amer. Phys. Soc. 25, 833 (1980).

10. A. Bernard, "Plasma Focus", Pulsed High Beta Plasmas, D. E. Evans, ed., (Pergamon Press, New York, 1976) 69.

11. M. J. Bernstein and G. G. Comisar, Phys. Fluid 15, 700 (1972).

12. N. V. Filippov and T. I. Filippova, JETP Lett. 25, 241 (1977).

13. R. P. Vasileva, M. I. Pergament, and A. I. Yaroslavsky, Nucl. Fusion, Spec. Suppl., 129 (1969).

14. Y. Kitagawa, Y. Yamada, A. Ishizaki, M. Naito, M. Yokoyama and C. Yamanka, 1980 IEEE Inter. Conf. on Plasma Sci. Conf. Rec.-Abstracts, IEEE Catalog No. 80CH1544-6 NPS, p. 74 (1980).

15. H. H. Andersen and J. F. Ziegler, Hydrogen Stopping Power and Ranges in All Elements, Vol. 3 of series. Stopping and Ranges of Ions in Matter, (Pergamon Press, New York, 1977).

16. B. Rossi and K. Greisen, Rev. Mod. Phys. 13, 240 (1941).

17. R. D. Evans, The Atomic Nucleus, (McGraw-Hill, 1955) p. 633-636.

18. S. P. M. Stier, C. F. Burnett, and G. E. Evans, Phys. Rev. 96, 973 (1954).

19. A. G. Hill, W. W. Buechner, J. S. Clark and J. B. Fisk, Phys. Rev. 55, 463 (1939) and N. Campbell, Phil. Mag 29, 783 (1915).

20. S. A. Goldstein and R. Lee, Phys. Rev. Lett. 35, 1079 (1975).

21. W. H. Bostick, V. Nardi, W. Prior, J. Feugeas, H. Kilio, C. Powell, Bull. Amer. Phys. Soc. 23, 848 (1978).

22. G. Gerdin, W. Stygar and M. Vernon, Conf. Record-Abstracts 1979 IEEE Int. Conf. on Plasma Sci., IEEE 79 CH1410-0 NPS, 111 (1979).

23. W. Stygar and G. Gerdin, Bull. Am. Phys. Soc. 24, 1039 (1979).

24. G. Gerdin, W. Stygar and F. Venneri, Conf. Record-Abstracts 1980 IEEE Int. Conf. on Plasma Sci., IEEE 80CH1544-6, 75 (1980).

25. I. F. Belyaeva, Nucl. Fusion, 20, 1037 (1980).

26. F. C. Young, J. Golden, and C. A. Kapetanakos, Rev. Sci. Instrum. 48, 432 (1977).

27. Instructions for the Use of CA80-15 Film and LR115 Film, Type I and Type II, Kodak, Kodalith and Wratten, France.

28. M. Varnagy, U. Szabo and S. Szegedi, Nucl. Instrum. and Meth. 154, 557 (1978).

29. R. H. Huddlestone and S. L. Leonard, Plasma Diagnostic Techniques (Academic Press, 1965) 8.

30. D. A. Hammer and N. Rostoker, Phys. Fluids 13, 1831 (1970).

31. L. Spitzer, Jr., Physics of Fully Ionized Gases, 2nd Ed., (Interscience, 1962) 143.

32. D. Pellinen, Rev. Sci. Instrum., 41, 1347 (1970).

33. W. A. Stygar, private communication.

34. J. D. Lawson, The Physics of Charged Particle Beams, (Oxford U. Press, 1977) 239.

35. G. I. Kotlyarevskii and Yu. P. Usov, Sov. Phys. Tech. Phys., 21, 887 (1976).

36. R. C. Davidson and N. A. Krall, Nucl. Fusion 17, 1313 (1977).

37. S. Maxon and J. Eddleman, Phys. Fluids 21, 1856 (1978).

38. J. W. Mather, Methods of Exp. Phys. 9B (Academic Press, 1971) 187.

39. W. A. Stygar, M.S. Thesis, University of Illinois (1980).

40. L. J. Demeter and V. L. Bailey, private communication

41. K. Hirano, K. Shimoda, and S. Emori, Rev. Sci. Instrum. 50, 1236 (1979).

42. B. D. Guenther, R. Lontz, J. T. May, and C. M. Stickley, Proc. of the Particle Beam Research Workshop, U.S. Air Force Academy, 18 (10-11 Jan. 1980).

Figure 1. Faraday cup, drift region and DPF configuration. The differential pumping hole is .476 cm long.

Figure 2. (a) Bias circuit.
(b) Faraday cup detail. B_1=500 G, B_2=100 G and B_3=100 G.
All magnetic fields are produced by permanent magnets (not shown).

Figure 3. Simultaneous signals from the (a) SPMT, (b) MIC (cup) and (c) SEE (grid). The ion flight path is 48 cm. The neutron yield for this shot was 2.3×10^9 (3 torr DPF fill gas, 12.5 kilojoule bank energy).

Figure 4. MIC and corresponding SPMT signals for shots taken 12 June 1980. The DPF fill gas is a mixture of 2 torr hydrogen and 2 torr deuterium; the ion flight path is 94 cm.

Figure 5. Time of flight ratios for the two SEE (cup) signal peaks as a function of average deuteron energy observed when using a DPF fill gas mixture of 2 torr hydrogen and 2 torr deuterium.

Figure 6. Schematic of neutron generator (Texas Nuclear) used in the feasibility irradiations of LR115 type II. The upper limit to the accelerator acceleration energy is 150 keV at 1mA.

Figure 7. Microscopic view of LR115 type II around a 0.36 mm diameter hole in the copper plate (figure 6). The target was irradiated by a 150 keV, 5-6μA deuteron beam for 120 seconds. The etch conditions were 2.5N KOH at 61°C for 40 minutes. These conditions resulted in a depth of surface removed of 3.7μm and a mean track diameter of 12μm.

Figure 8. The LR115 detectors were irradiated in the configuration shown. Target A is LR115 type II with the $Li_2B_4O_7$ layer. Target B is LR115 type I covered with 1.5 mil of Ł mylar and Target C is LR115 type I covered with 2.0 mil of mylar.

Figure 9. The energy of the emergent deuterons (vertical axis) versus their incident energy (horizontal axis) after traveling through various thicknesses of mylar (solid lines). The dotted line is a similar curve for 100μm of $Li_2B_4O_7$ which is approximately the thickness of the converter layer in LR115 type II.

Figure 10. Microscopic view of LR115 type II around a 1mm diameter hole in the copper cover plate in area A (figure 8). The etch conditions are similar to those of figure 7 and the depth of surface removed by the etch was 5μm. The neutron yield on this shot was 3.8×10^9 [D(d,n)^{3}He], the fill pressure was 3.0 torr D_2, and the bank energy 11.5kJ (bank voltage 24 kV).

Figure 11. Microscopic view of LR115 type I covered by 1.5 mil mylar around a 1mm diameter hole in the copper cover plate in area B (figure 8). The etch conditions and depth of the surface removed are the same as in figure 10. The DPF shot was the same as in figure 10.

Figure 12. Microscopic view of LR115 type I covered by 2.0 mil mylar around a 1mm diameter hole in the copper cover plate in area C(figure 8). The etch conditions and depth of the surface removed are the same as in figure 10. The DPF shot was the same as in figure 10.

Figure 13. Microscopic view of unirradiated LR115 type II used to evaluate the background. The etch conditions were 2.5 N KOH at 60°C for 40 minutes and the depth of the surface removed was 4.8μm.

Figure 14. Data showing correlation of neutron yield with net electron current in 1.5 torr deuterium. Symbols: 0 no nitrogen added, Δ: 50μ of nitrogen added and X: 200μ of nitrogen added.

Figure 15. Simultaneous signals from the electron Rogowski coil and scintillator-photomultiplier tube where the sharp peaks near the end of both signals are a time marker. The thermocouple is attached to a lead target and the scintillator has been shielded by a combination of lead, paraffin and cadmium so only X rays (no neutrons) with energies greater than 100 keV coming from the lead target can be observed.

Figure 16. Plot of net electron current for the best shots at each voltage versus mainbank voltage for hydrogen gas. The arrows point to voltages where I_{net} stops increasing with bank voltage, V_{BRK}.

Figure 17. Comparison of measured run in times with those calculated from snow plow model normalized for increasing bank voltage at 3 torr in hydrogen. When the net current stops increasing there is some evidence that a minimum in the measured run in time has been reached.

Figure 18. Plot of voltage when I_{net} stops increasing vs pressure (Figure 16). A slope of six would agree with the model for breakdown of gas behind the current sheath caused by high impedance coaxial electrodes when the sheath velocity is too high.

Figure 19. Scaling of I_{net} electron current with mainbank current for mainbank voltages less than 19 kV (Figure 16).

Figure 20. A schematic view of the high current fast Faraday cup to measure the primary electron current along with a signal taken during a DPF shot. Areas represented by (a) are evacuated to about 0.04 torr to increase the voltage standoff, (b) represents the mylar foil used to provide insulation between the cup (c) and the shunt (d). A 5 mil mylar foil (e) prevents plasma return currents.

Figure 21. A schematic view of the electron magnetic spectrometer and its connection to the DPF itself. (a) is the hollow DPF center electrode, (b) and (c) represent the 4.5 cm ID aluminum drift tube which is at the fill pressure of the DPF (3.0 torr D_2). (d) is the beam dump, (e) the fringe field shield (Armco), (f) the collimators and (g) are the Faraday cups which are connected to the screen room by 5 meters of 50Ω cable in a braided conduit.

Figure 22. Simultaneous signals observed on two channels of the magnetic spectrometer (figure 21) during a DPF shot. The negative trapezoidal pulse at the beginning of both signals is a time marker.

Figure 23. Time integrated electron beam energy spectra four separate DPF shots represented by dashes, circles, lines and X's respectively. The data were normalized to the lowest energy channel (47 to 74 keV) and so only a flat horizontal line at $dN/dE_e = 10^3$ is used to represent this normalization. The line is a power law fit to these data with a slope of -3.6.

Figure 24. Simultaneously recorded ion energy and electron energy spectra. The ion energy spectra were evaluated using the scintillator photomultiplier tube and ion Faraday cup signals in time-of-flight analysis. The electron energy spectra are from four time-integrated channels of the electron magnetic spectrometer. The straight lines are power law fits to the ion and electron spectra where the exponents are -3.5 and -3.8 respectively.

Figure 25. Schematic diagram of the soft-Xray spectrometer-DPF system. The numbers designate the following components of the system: 1) adaptor flange, 2) Beryllium window, 3) steel bellows, 4) aluminum cylinder with pump-out tube, 5) Plexiglas insulator extension, 6) Plexiglas insulator, 7) and 10) tantalum collimators, 8) and 11) lead shields, 9) and 12) aluminum enclosures, 13) PIN diodes and 14) dense focused plasma.

Figure 26. The run-in time of the current sheath as measured at the point where the main current sharply decreases (figure 28) versus $\rho^{\frac{1}{4}} V^{-\frac{1}{2}}$ where ρ is the mass density of the filling gas and V is the mainbank voltage. The solid line is the prediction of the snowplow model.[38]

Figure 27. Plot of neutron yield versus mainbank current at pinch time. Filling pressure: 3 torr deuterium, bank voltage 16-24 kV.

Figure 28. Waveform of the mainbank current as observed on the mainbank Rogowski coil.

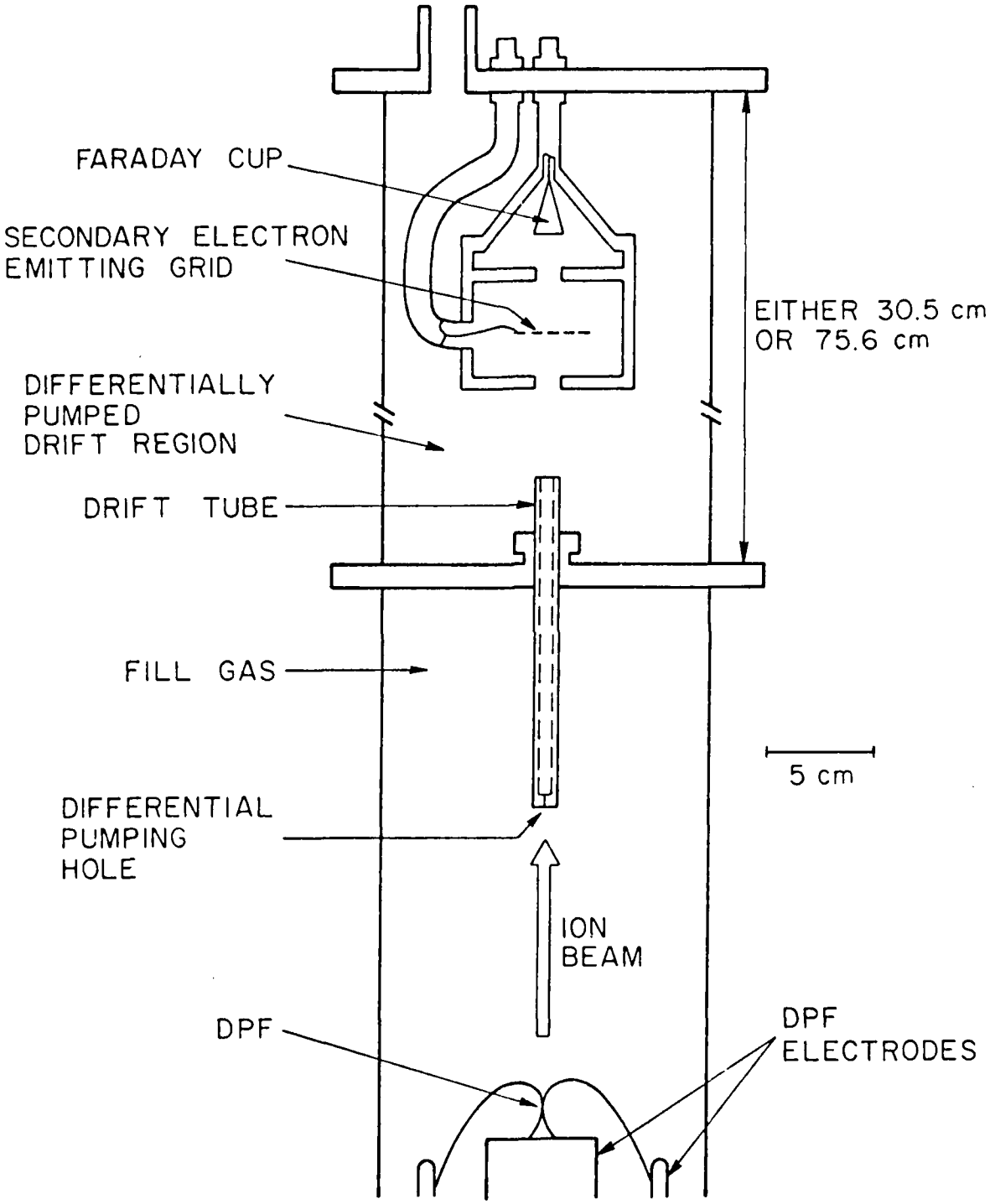
FARADAY CUP
SECONDARY ELECTRON EMITTING GRID
EITHER 30.5 cm OR 75.6 cm
DIFFERENTIALLY PUMPED DRIFT REGION
DRIFT TUBE
FILL GAS
5 cm
DIFFERENTIAL PUMPING HOLE
ION BEAM
DPF
DPF ELECTRODES

Figure 1

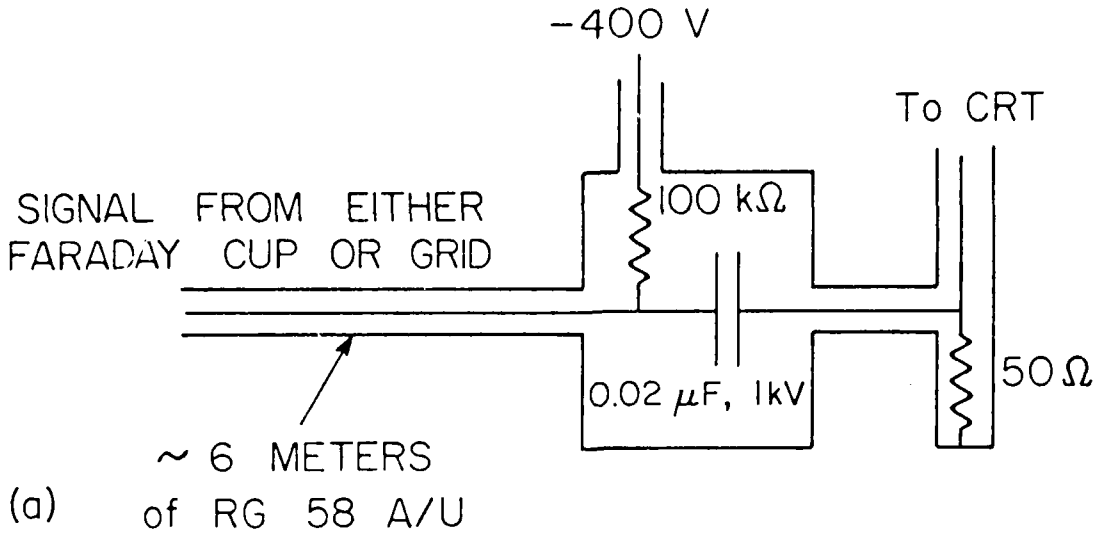
-400 V
To CRT
SIGNAL FROM EITHER
FARADAY CUP OR GRID
100 kΩ
0.02 μF, 1kV
50 Ω
~ 6 METERS
of RG 58 A/U

(a)

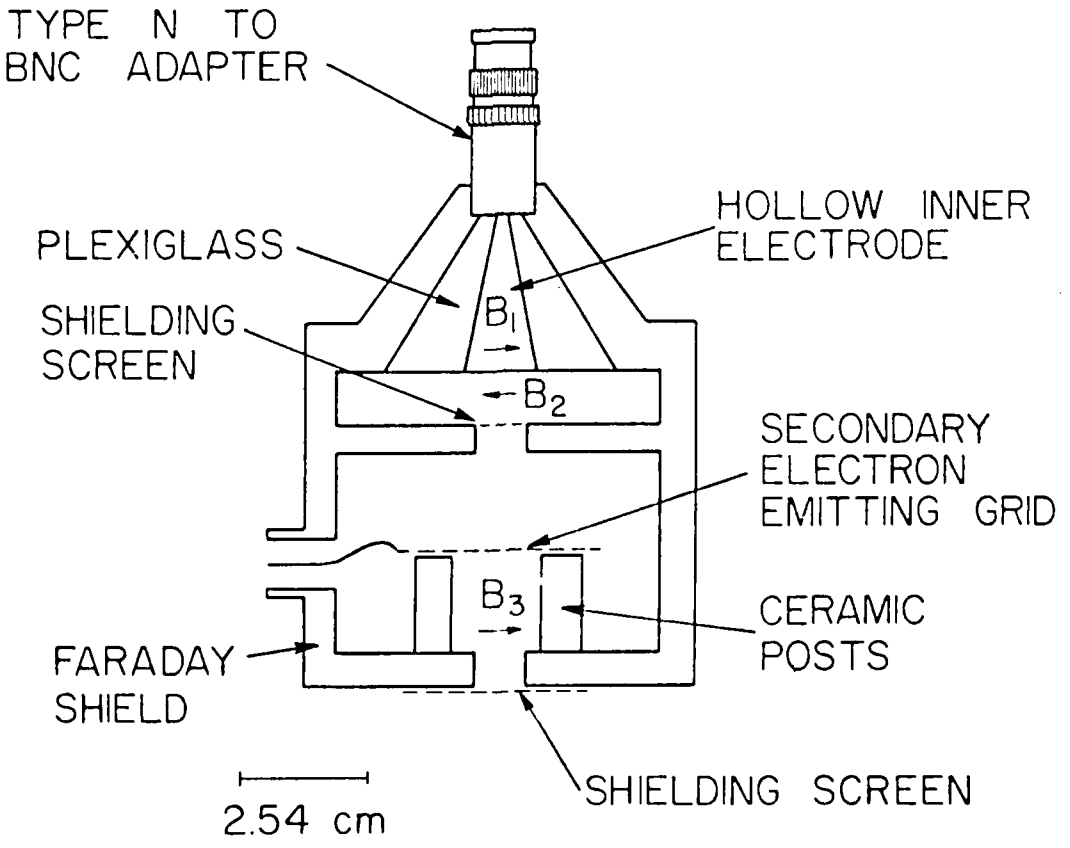
TYPE N TO
BNC ADAPTER
HOLLOW INNER
ELECTRODE
PLEXIGLASS
SHIELDING
SCREEN
B1
B2
SECONDARY
ELECTRON
EMITTING GRID
B3
CERAMIC
POSTS
FARADAY
SHIELD
SHIELDING SCREEN
2.54 cm

(b)

Figure 2

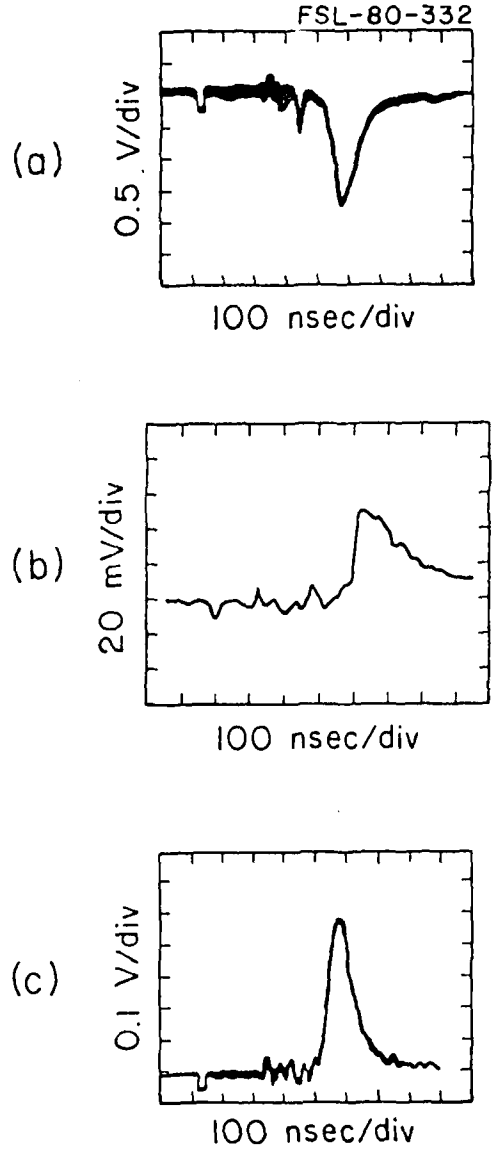
FSL-80-332
(a)
0.5 V/div
100 nsec/div
(b)
20 mV/div
100 nsec/div
(c)
0.1 V/div
100 nsec/div

Figure 3

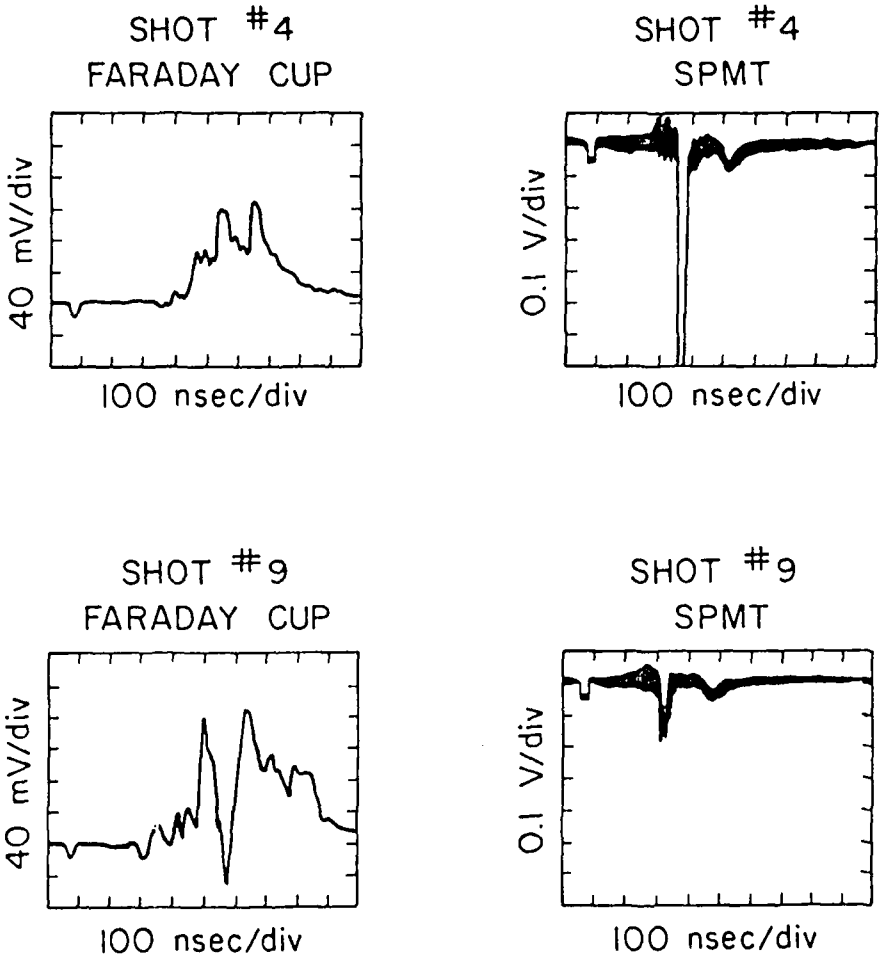
SHOT #4
FARADAY CUP
40 mV/div
100 nsec/div
SHOT #4
SPMT
0.1 V/div
100 nsec/div
SHOT #9
FARADAY CUP
40 mV/div
100 nsec/div
SHOT #9
SPMT
0.1 V/div
100 nsec/div

Figure 4

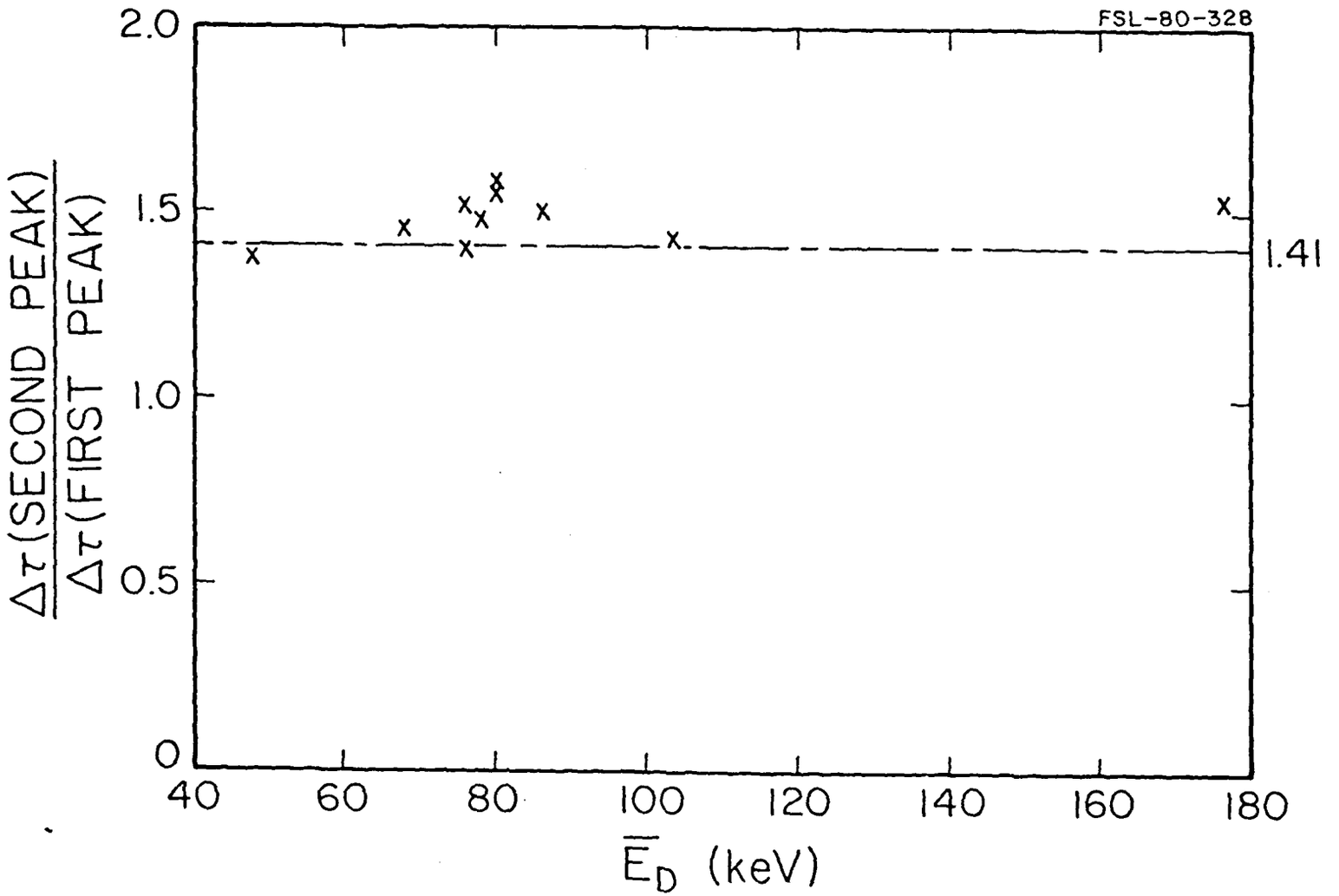
FSL-80-328
2.0
1.5
1.0
0.5
0
1.41
40
60
80
100
120
140
160
180
$\frac{\Delta\tau(\text{SECOND PEAK})}{\Delta\tau(\text{FIRST PEAK})}$
$\overline{E}_D$ (keV)

Figure 5

FSL-80-412

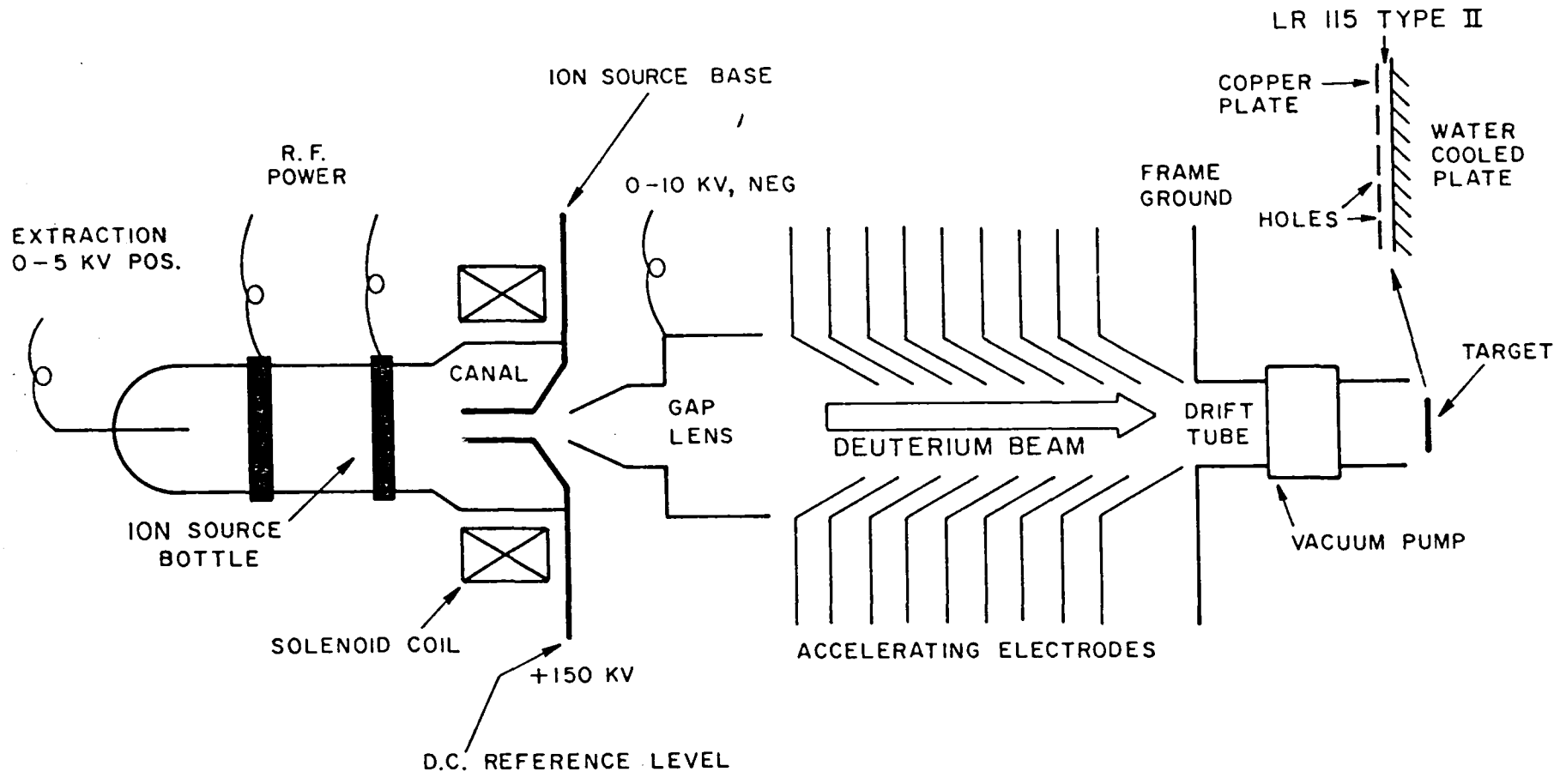

Figure 6

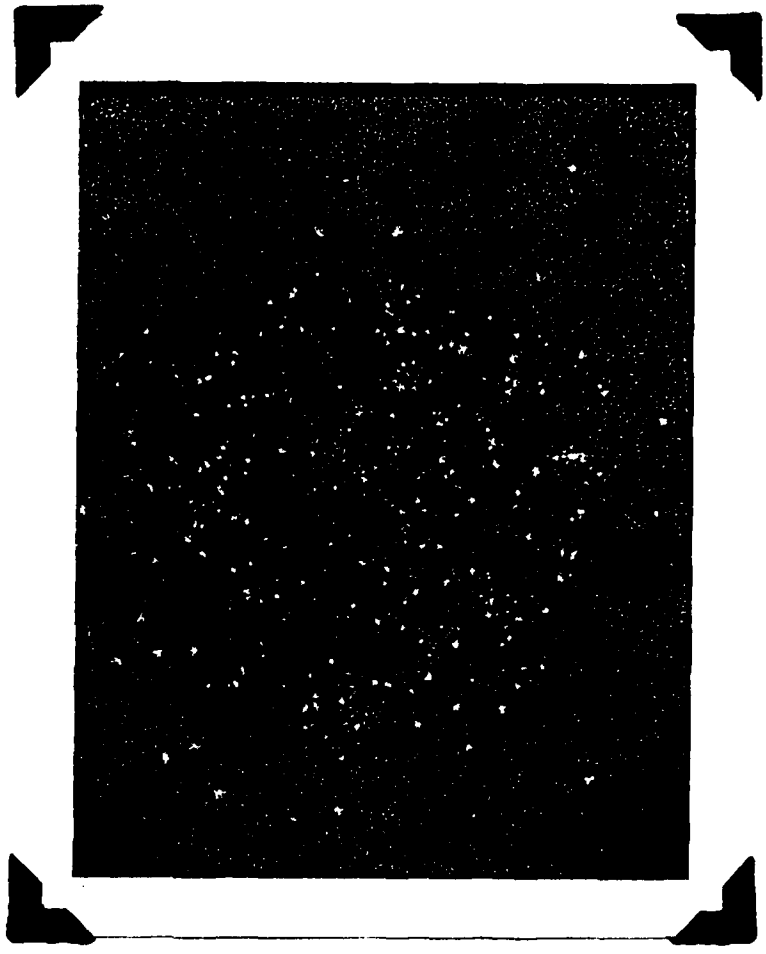

Figure 7

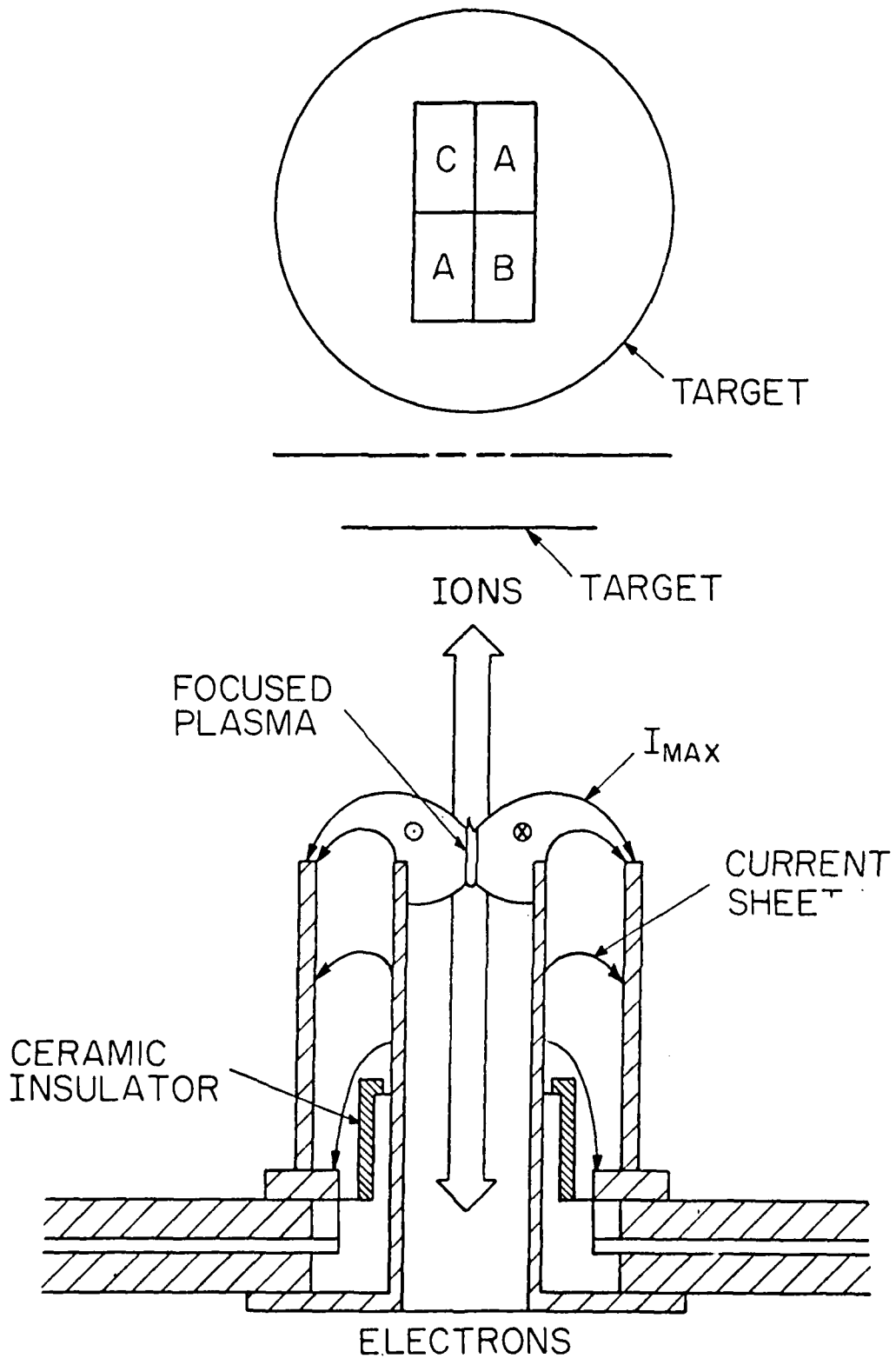
C
A
A
B
TARGET
IONS
TARGET
FOCUSED
PLASMA
I_{MAX}
CURRENT
SHEET
CERAMIC
INSULATOR
ELECTRONS

Figure 8

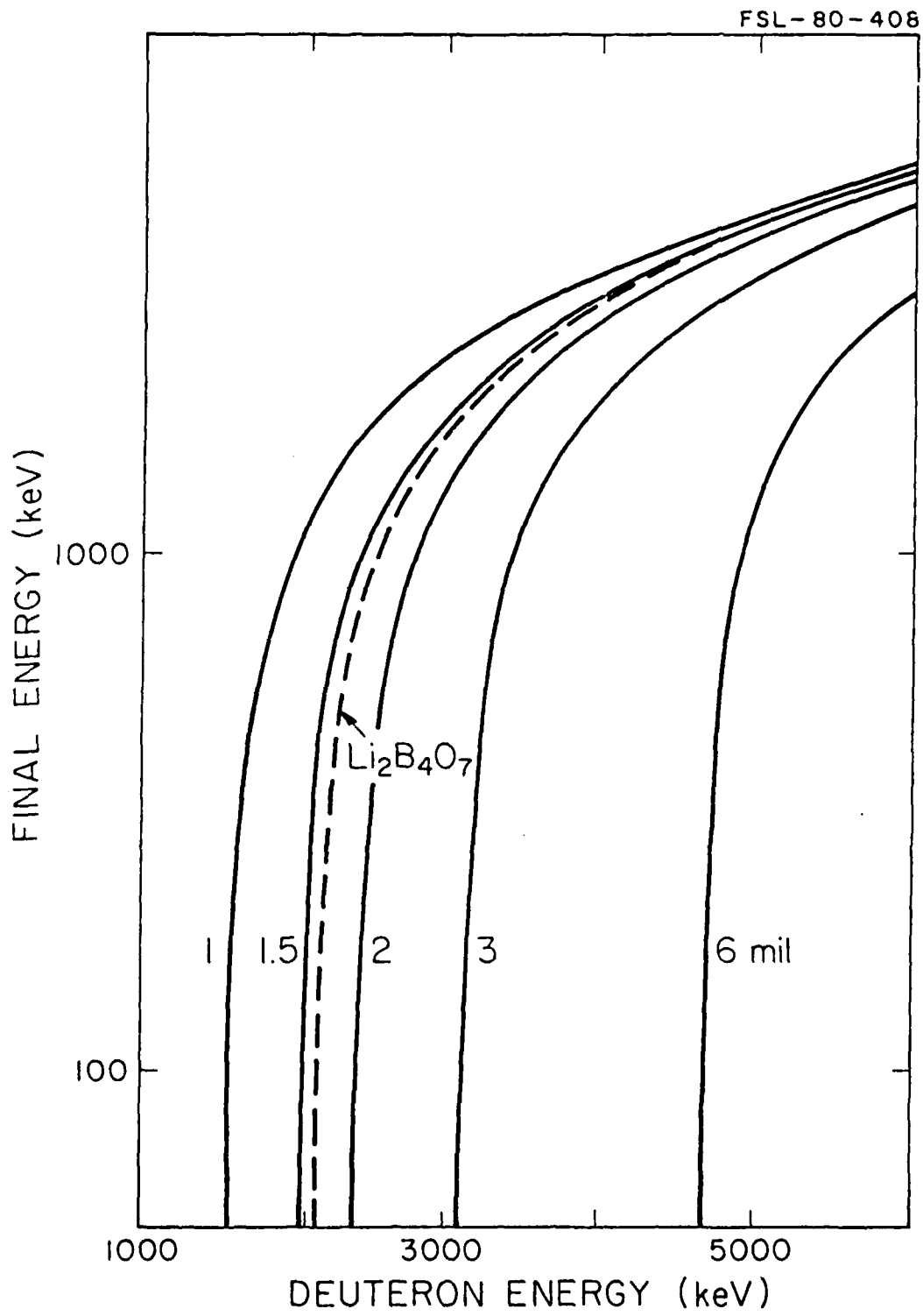
FSL-80-408
FINAL ENERGY (keV)
1000
100
1000
3000
5000
DEUTERON ENERGY (keV)
$Li_2B_4O_7$
1
1.5
2
3
6 mil

Figure 9

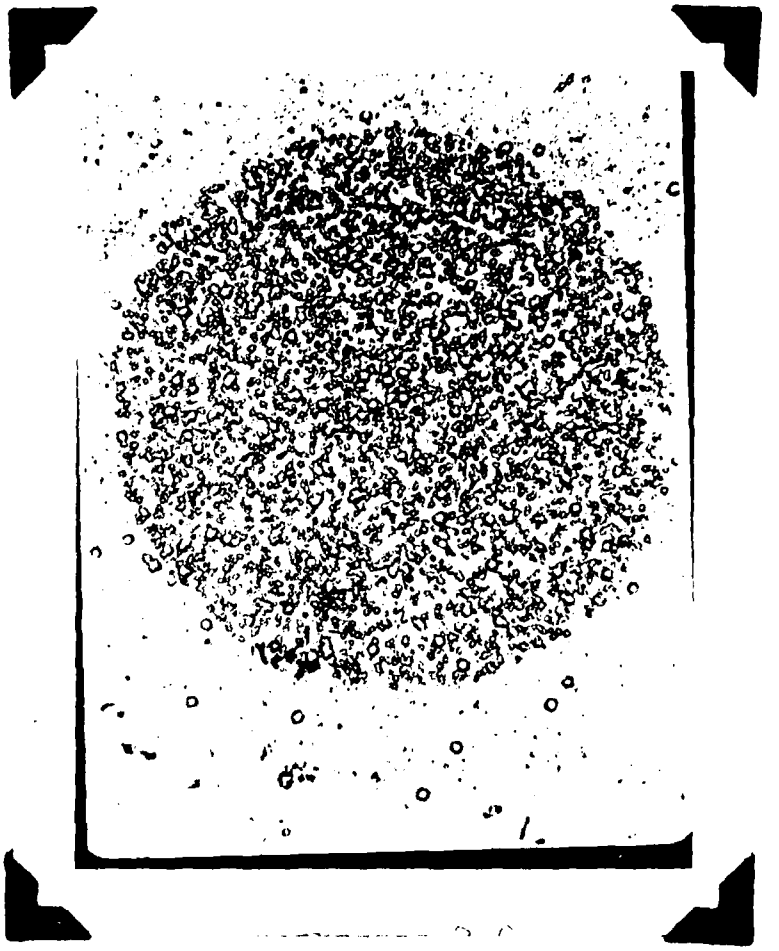

Figure 10

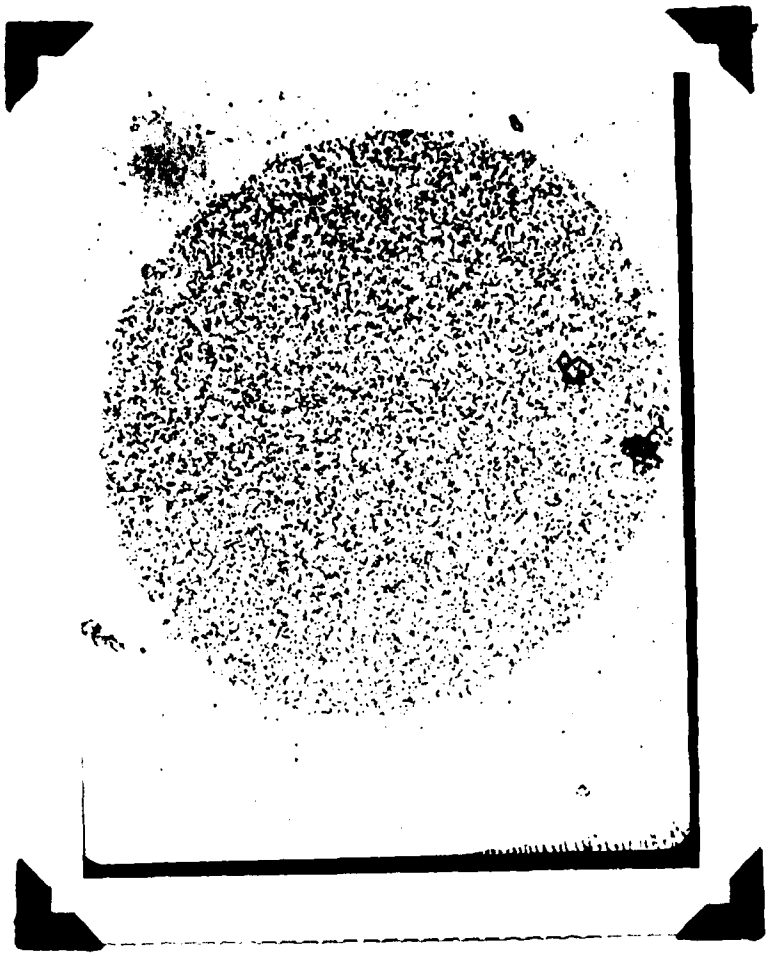

Figure 11

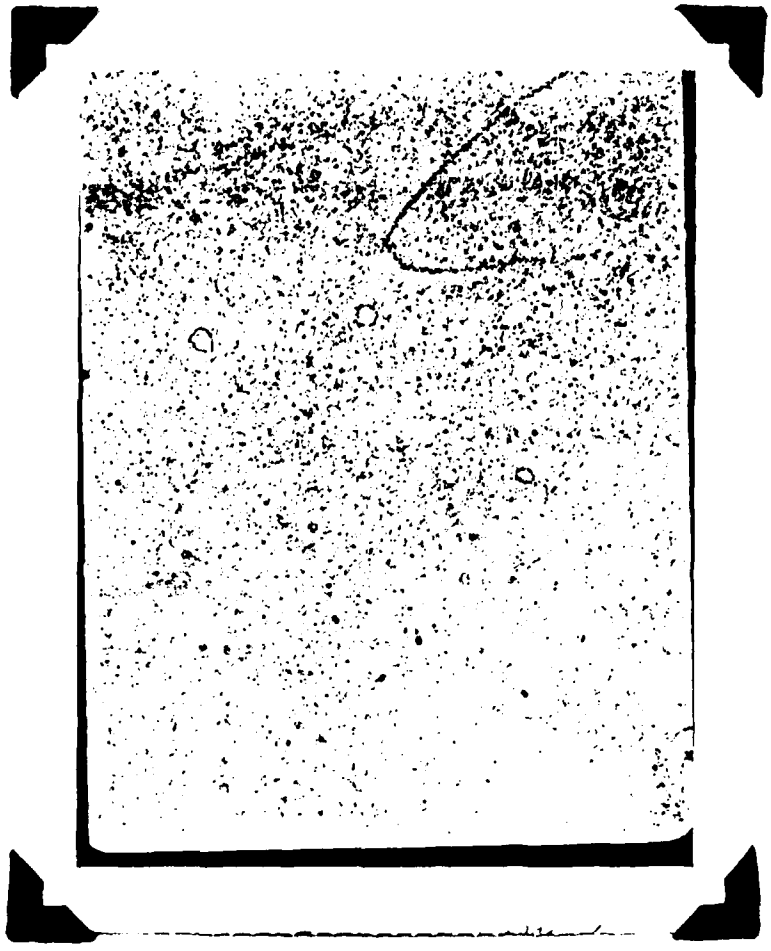

Figure 12

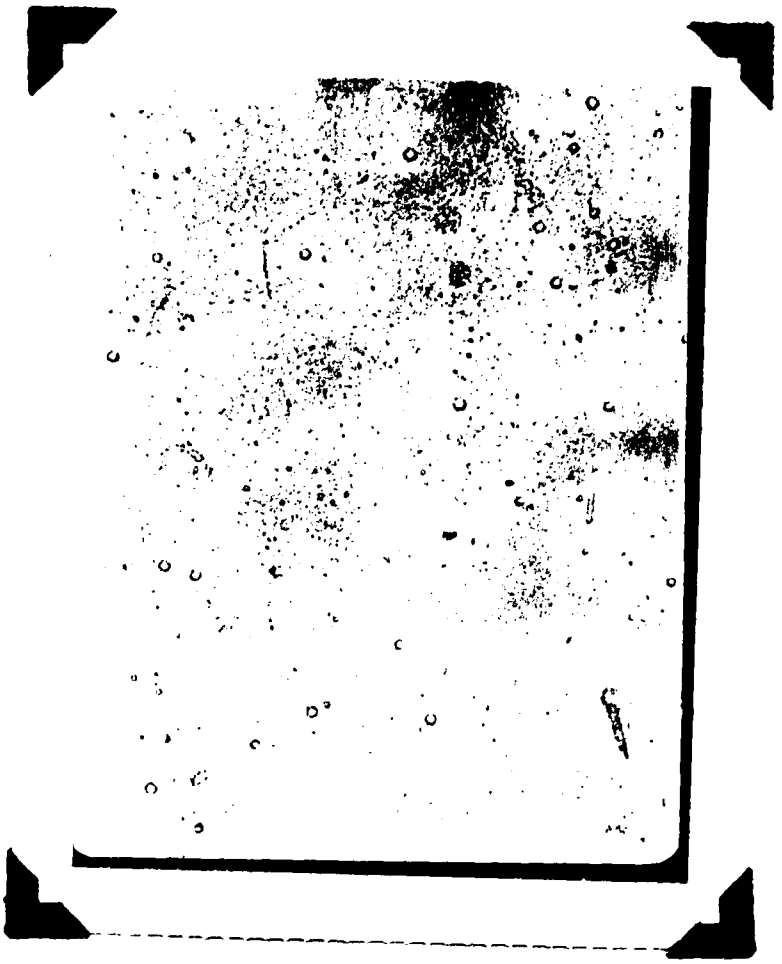

Figure 13

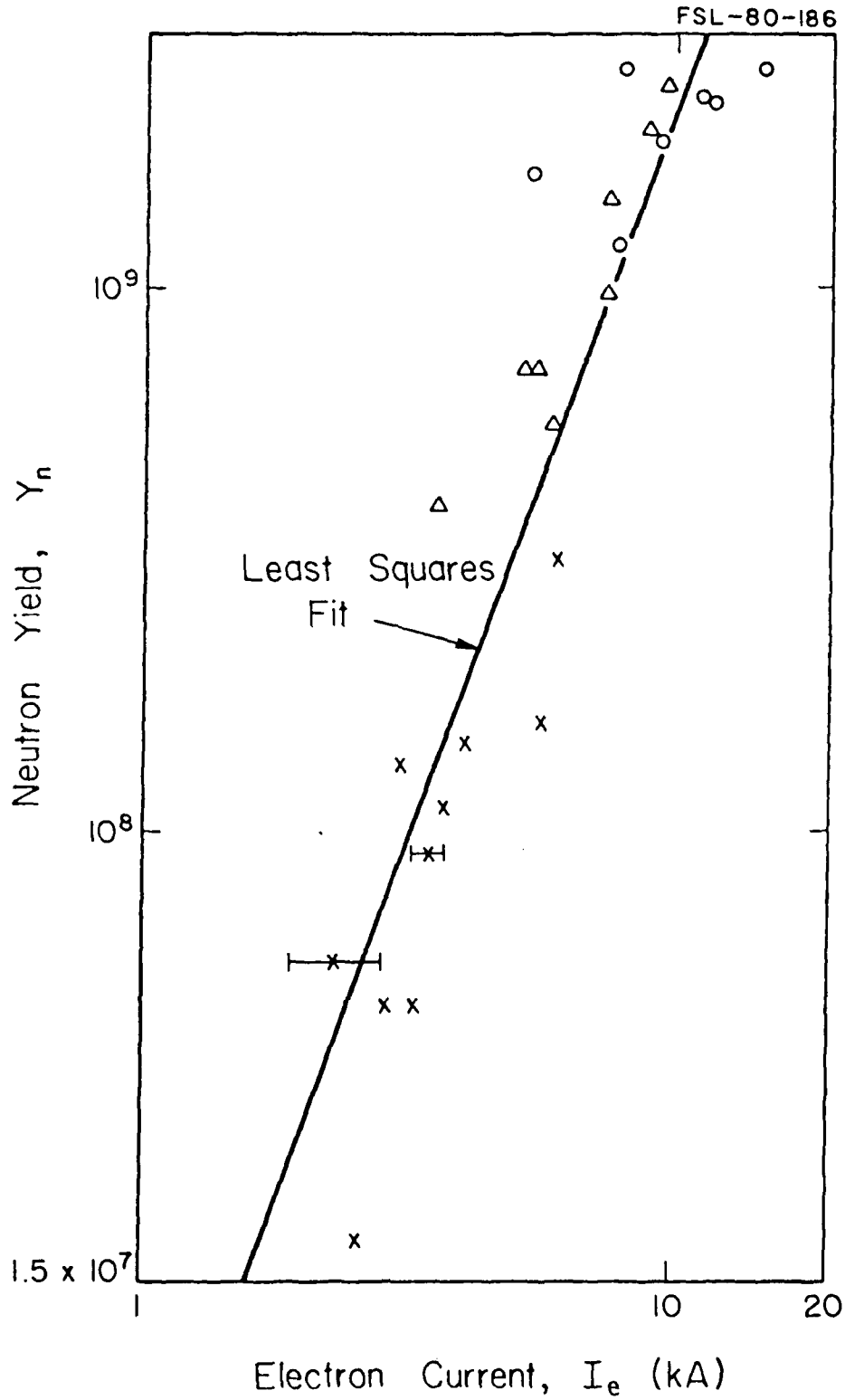
FSL-80-186
Neutron Yield, Y_n
10^9
10^8
1.5×10^7
Least Squares Fit
1
10
20
Electron Current, I_e (kA)

Figure 14

FSL-80-413

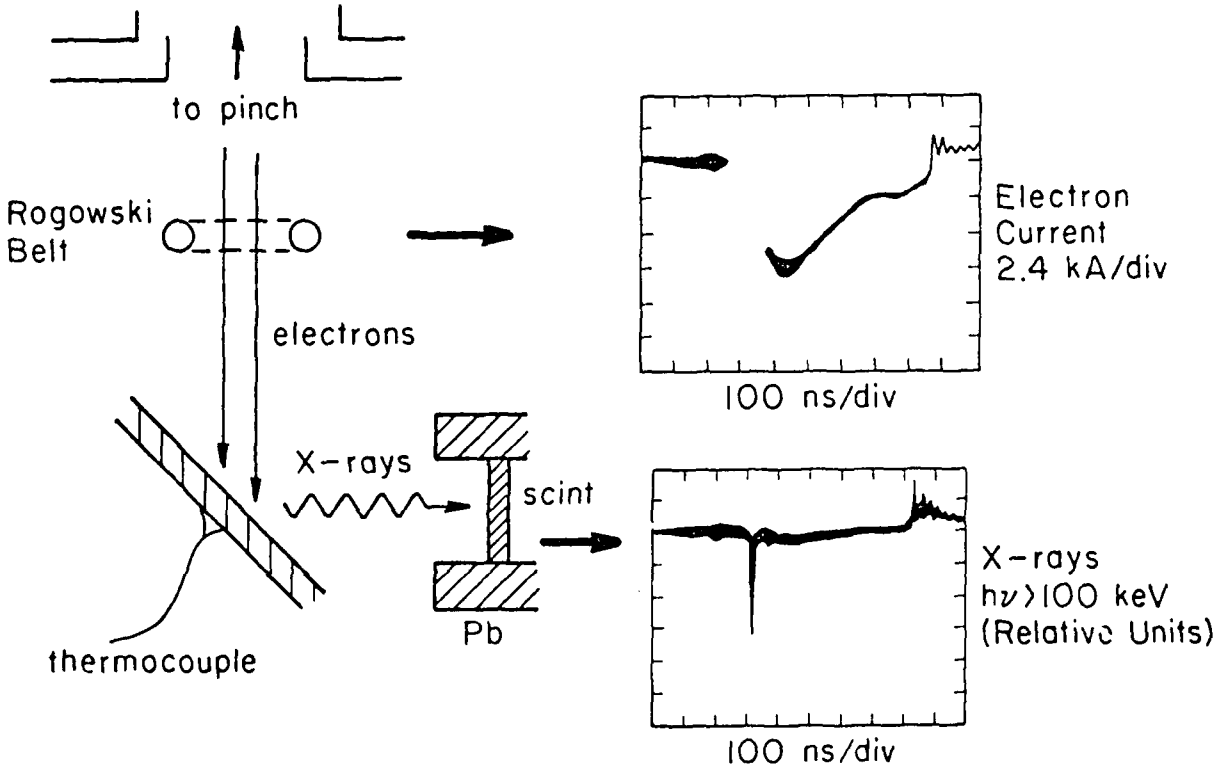

Figure 15

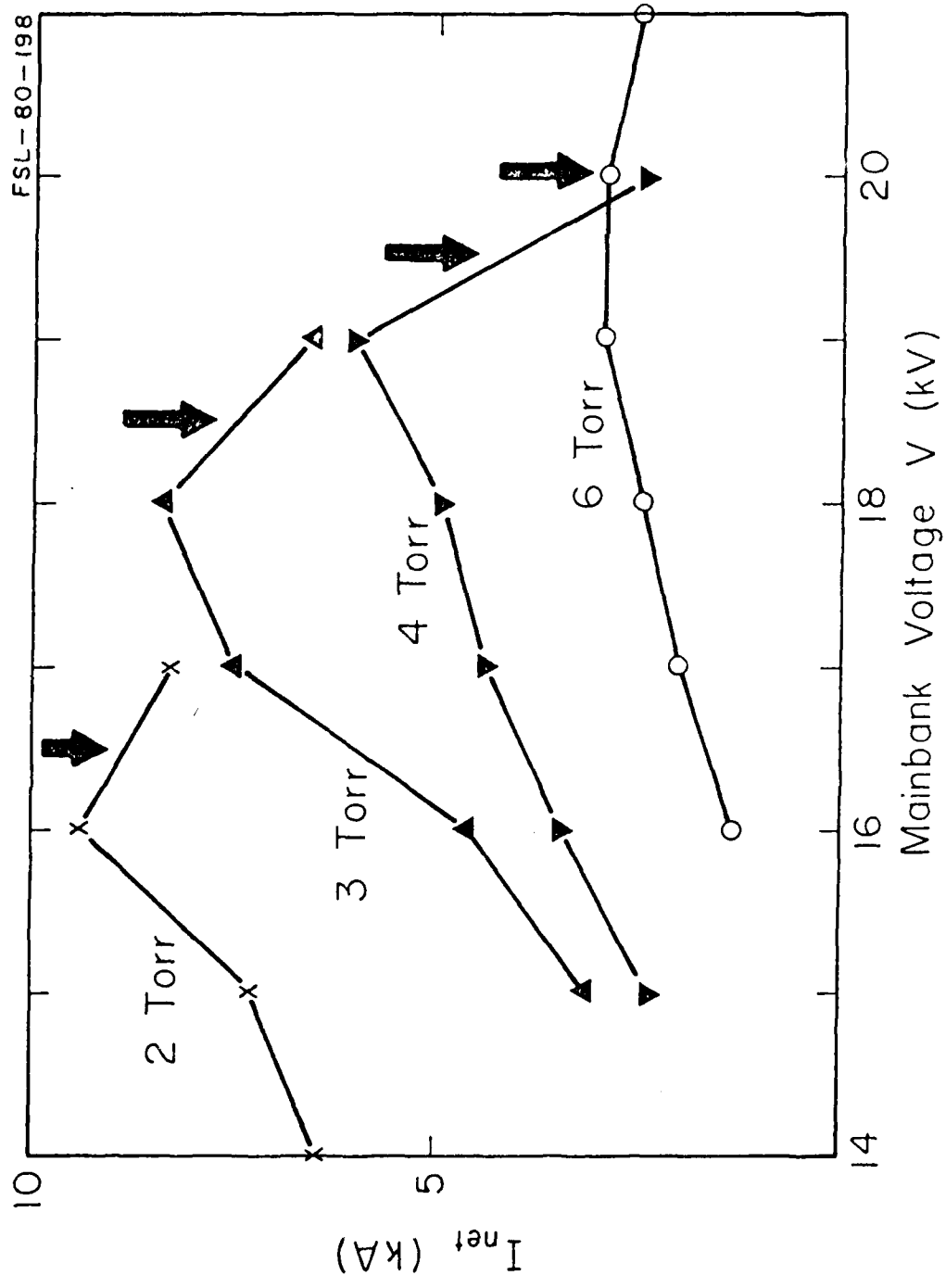
FSL-80-198
I_{net} (kA)
10
5
14
16
18
20
Mainbank Voltage V (kV)
2 Torr
3 Torr
4 Torr
6 Torr

Figure 16

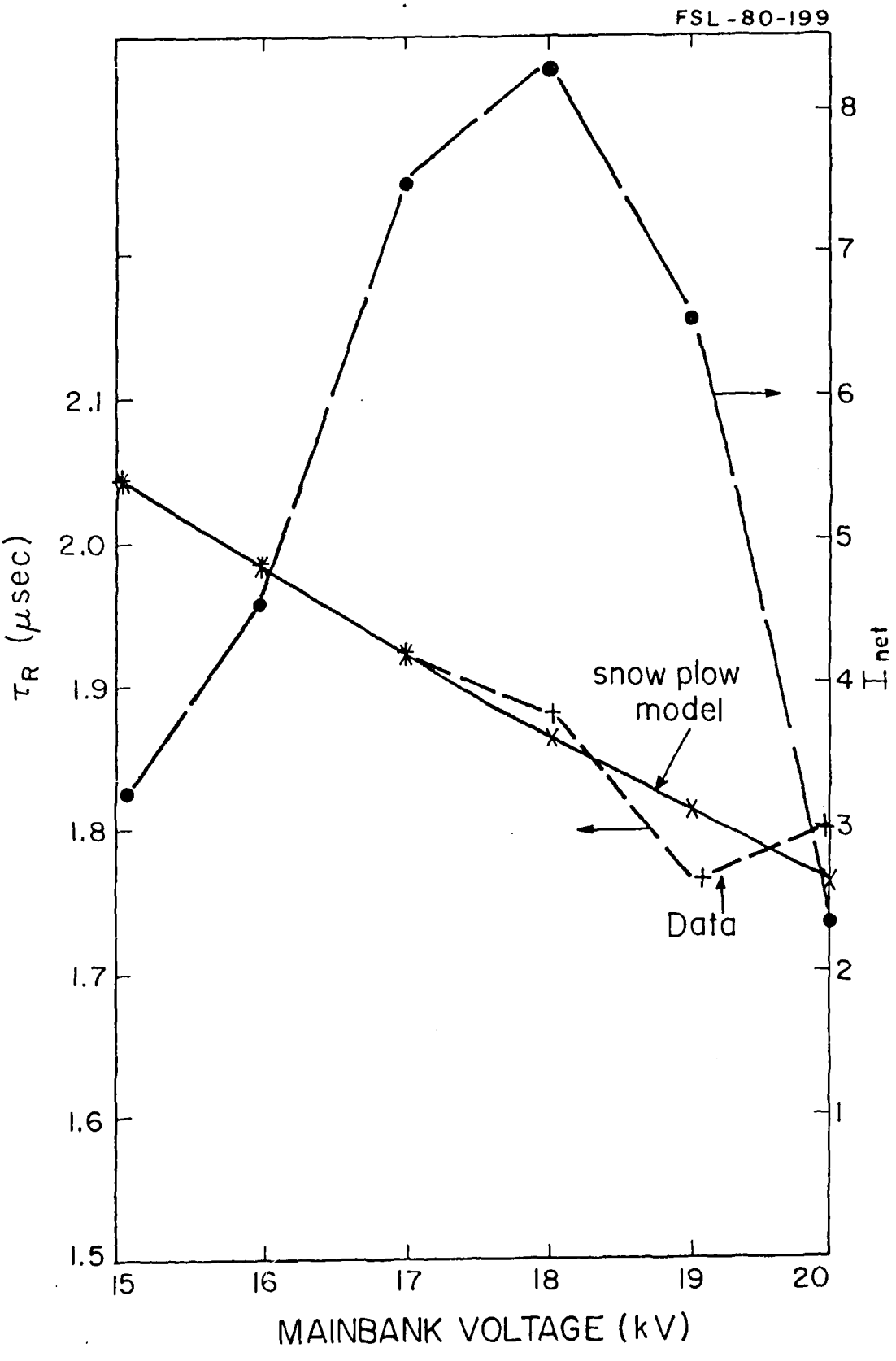
FSL-80-199
2.1
2.0
1.9
1.8
1.7
1.6
1.5
τ_R (μsec)
8
7
6
5
4
3
2
1
I_{net}
snow plow model
Data
15
16
17
18
19
20
MAINBANK VOLTAGE (kV)

Figure 17

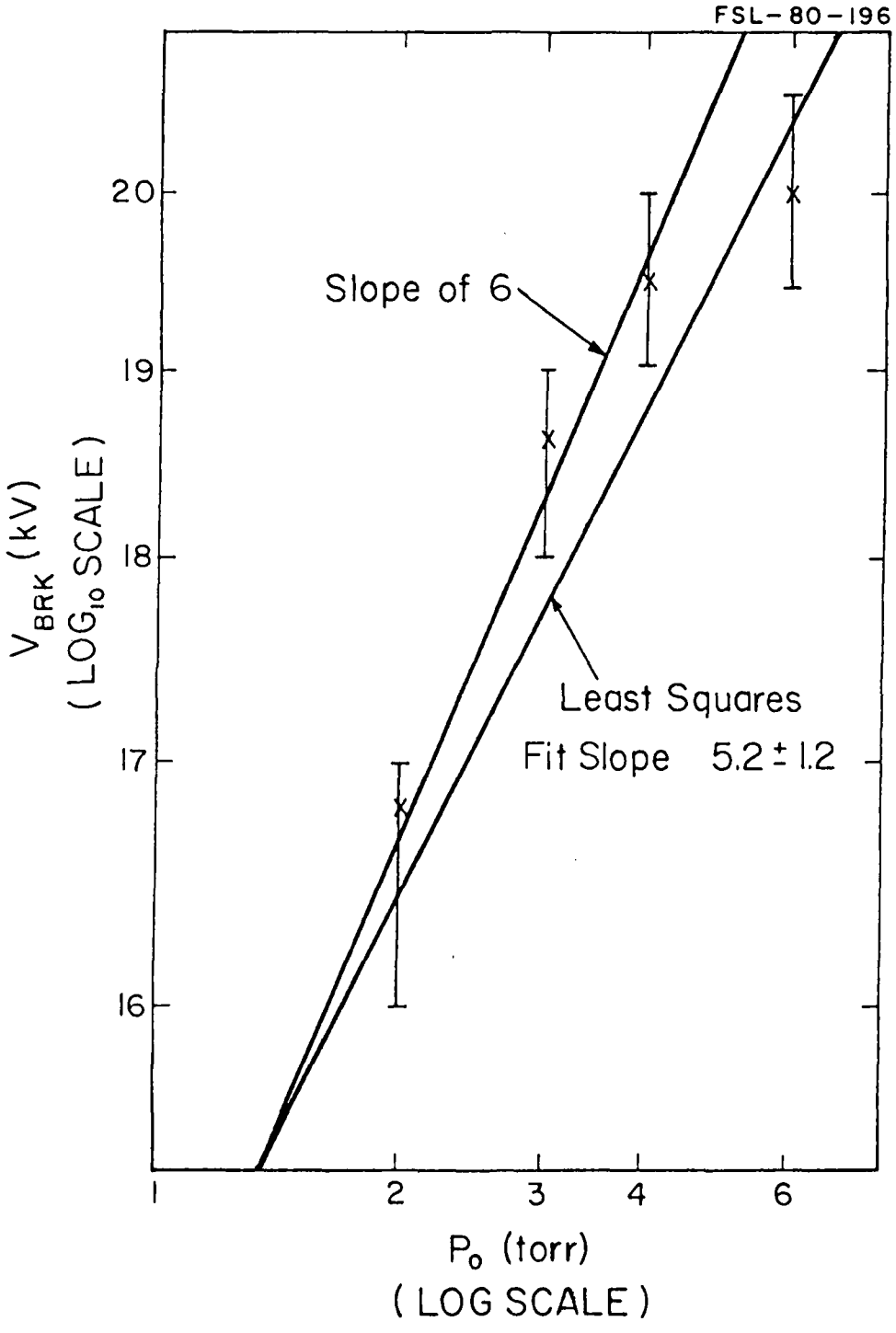
FSL-80-196
20
19
18
17
16
Slope of 6
Least Squares
Fit Slope 5.2 ± 1.2
V_{BRK} (kV)
(LOG_{10} SCALE)
1
2
3
4
6
P_o (torr)
(LOG SCALE)

Figure 18

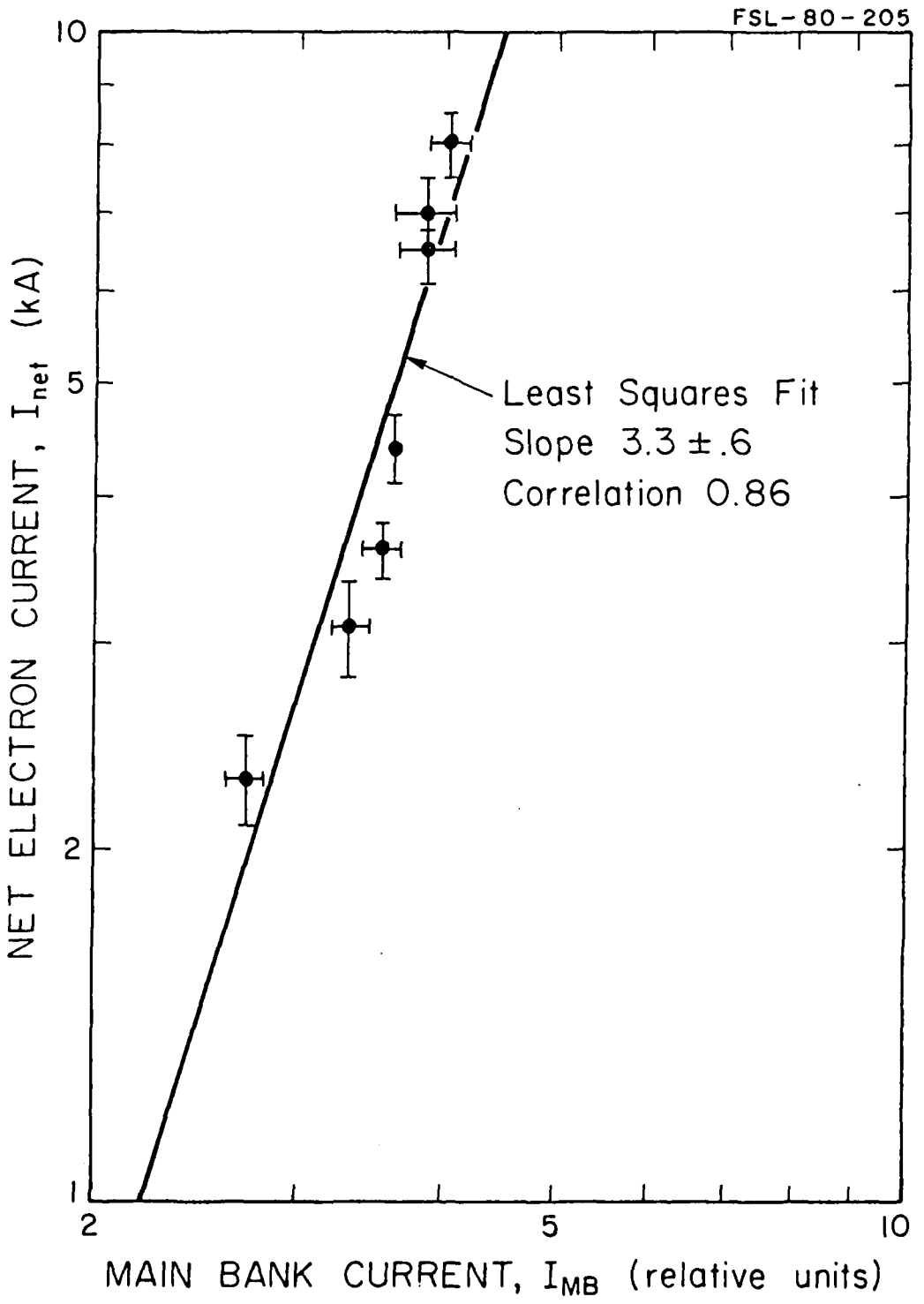
FSL-80-205
10
5
2
1
NET ELECTRON CURRENT, I_{net} (kA)
Least Squares Fit
Slope 3.3 ± .6
Correlation 0.86
2
5
10
MAIN BANK CURRENT, I_{MB} (relative units)

Figure 19

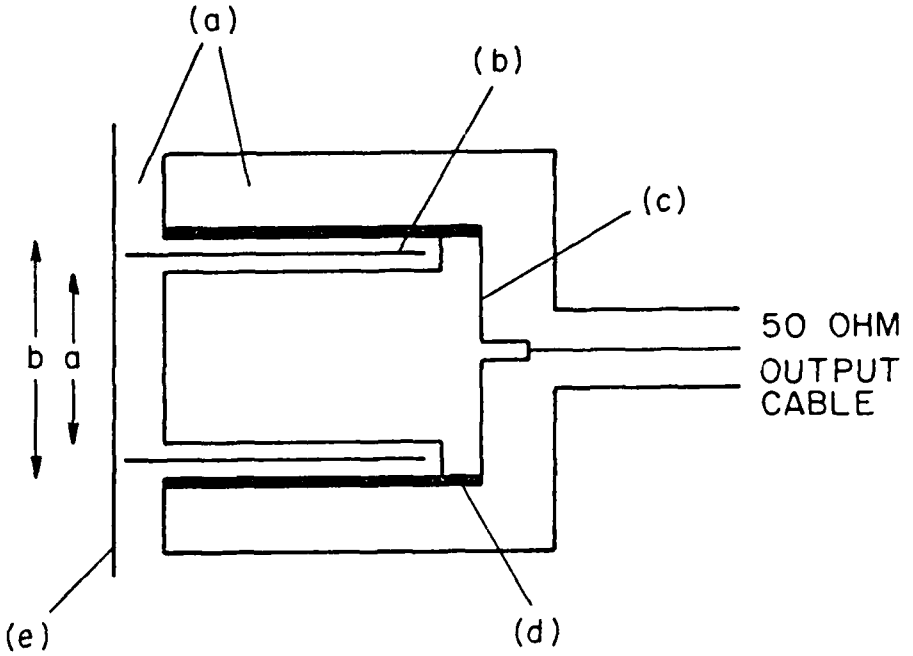

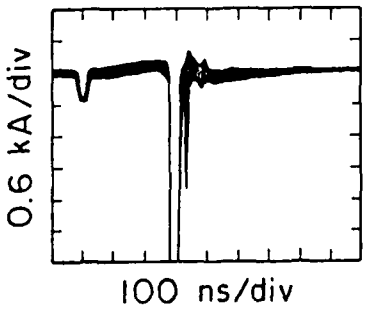

Figure 20

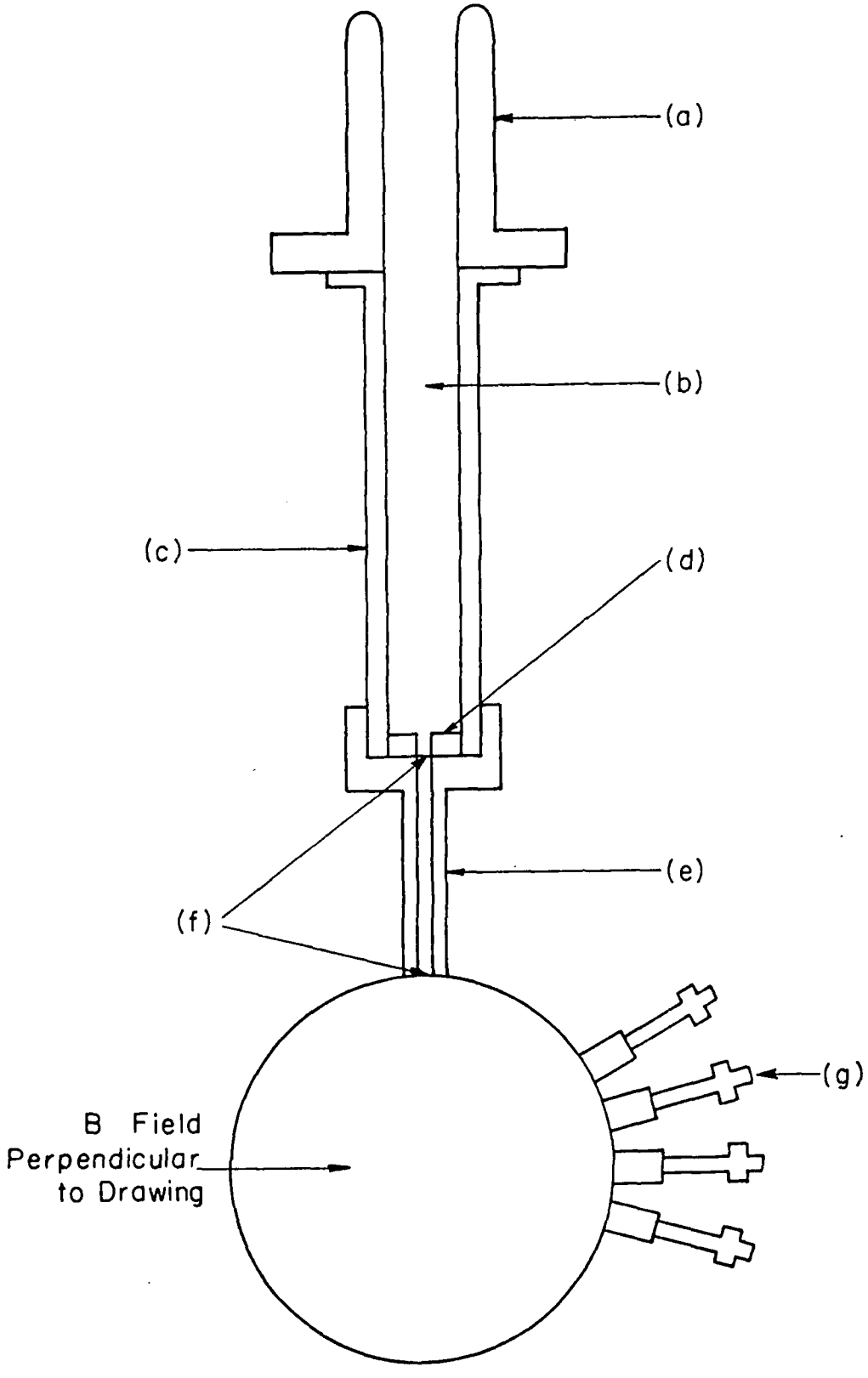

Figure 21

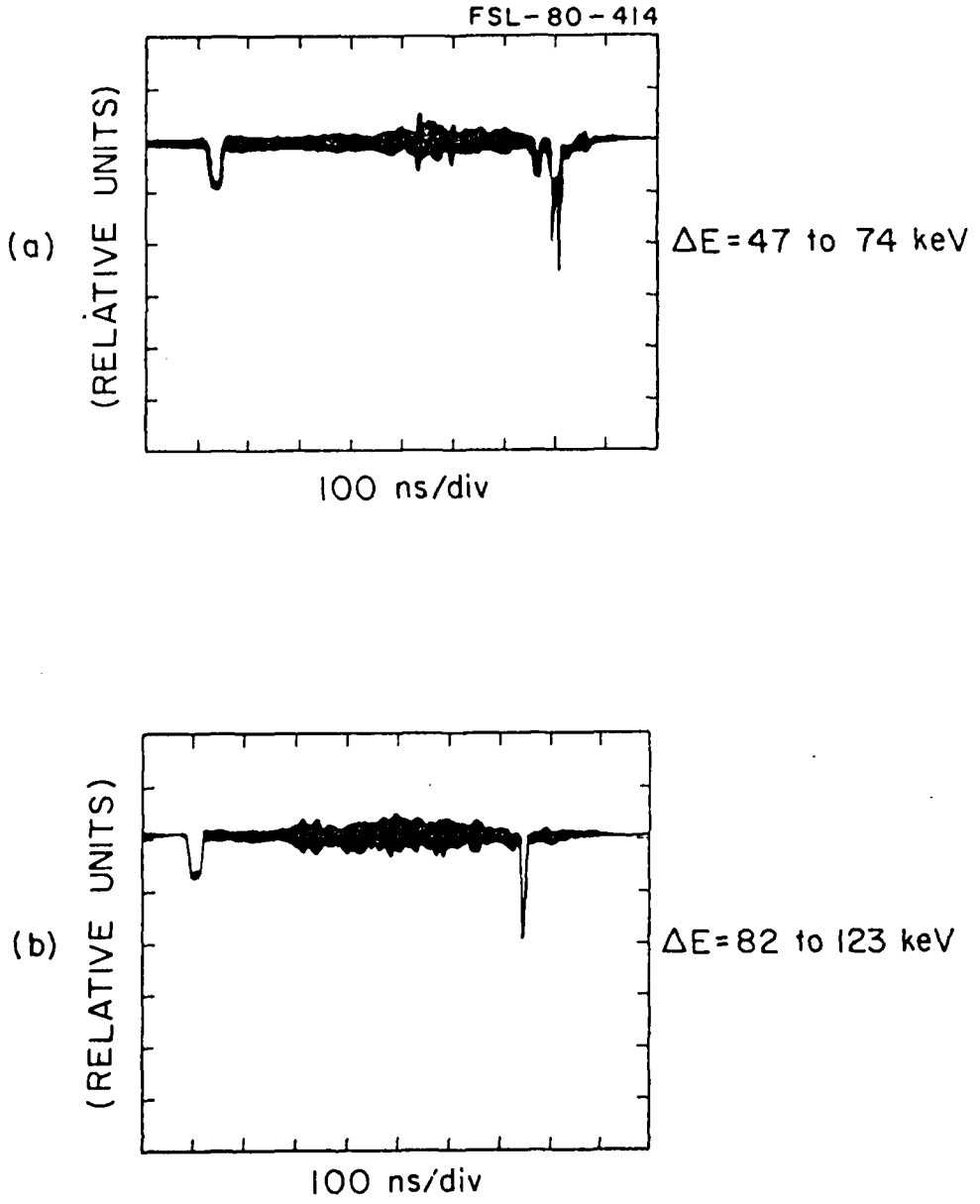
FSL-80-414
(a)
(RELATIVE UNITS)
ΔE=47 to 74 keV
100 ns/div
(b)
(RELATIVE UNITS)
ΔE=82 to 123 keV
100 ns/div

Figure 22

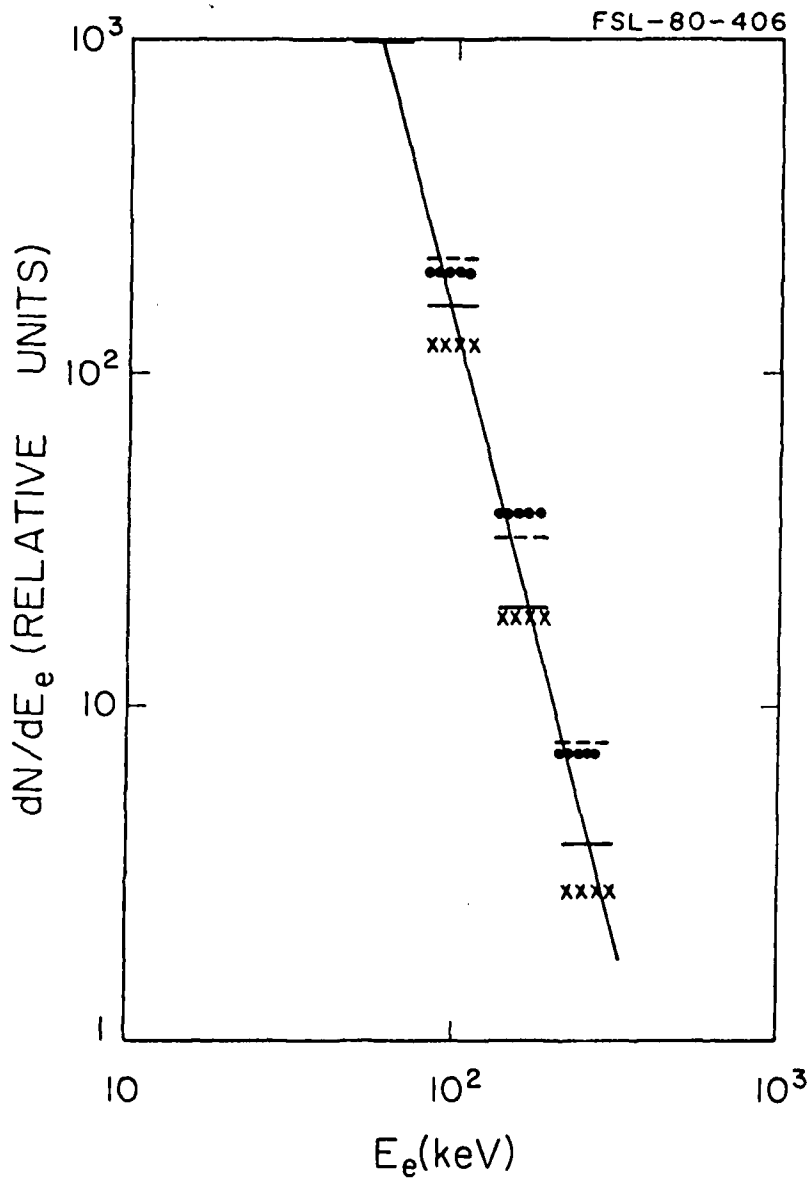
FSL-80-406
10^3
10^2
10
1
dN/dE$_e$ (RELATIVE UNITS)
xxxx
xxxx
xxxx
10
10^2
10^3
E$_e$(keV)

Figure 23

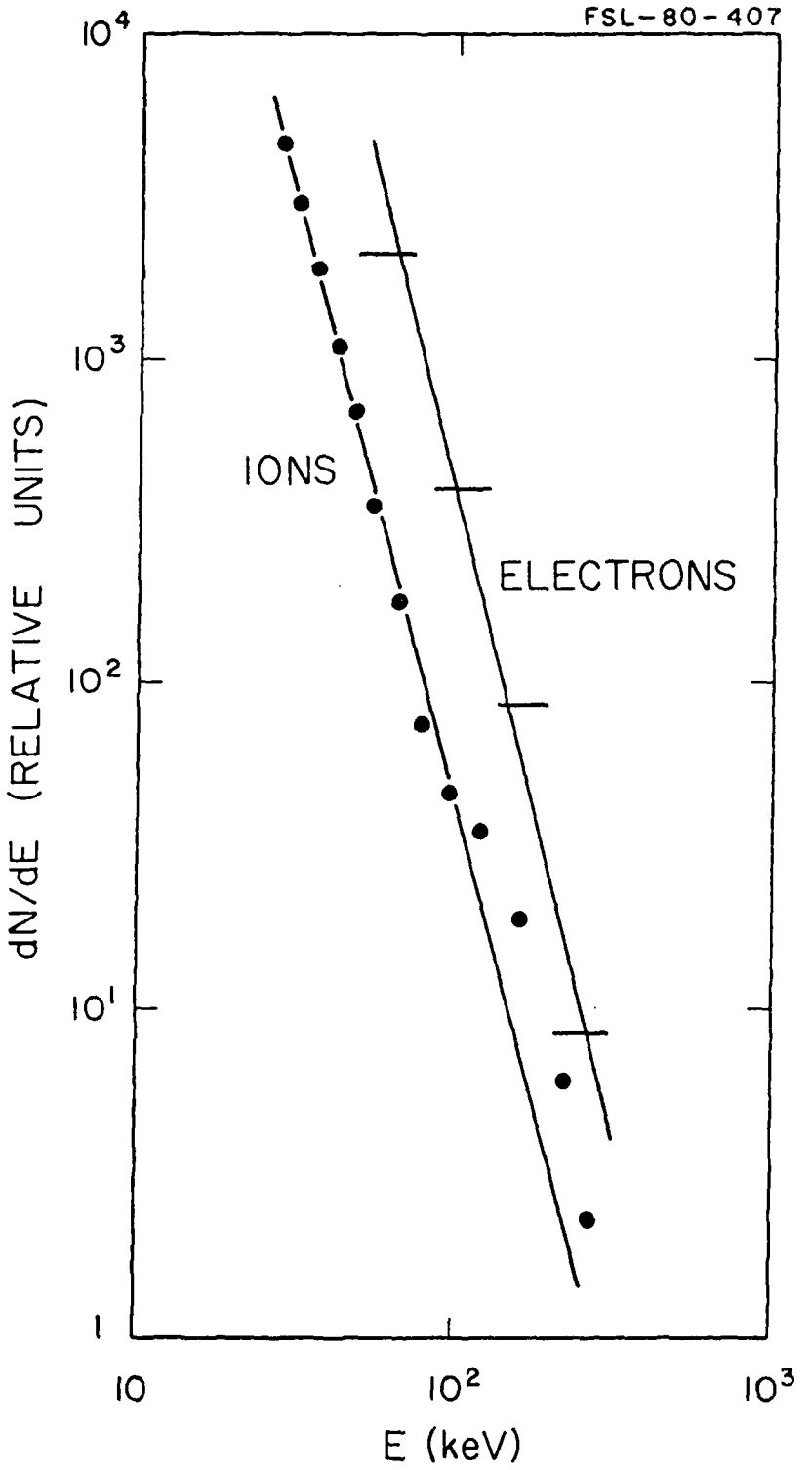
FSL-80-407
10^4
10^3
10^2
10^1
1
dN/dE (RELATIVE UNITS)
IONS
ELECTRONS
10
10^2
10^3
E (keV)

Figure 24

FSL-80-411

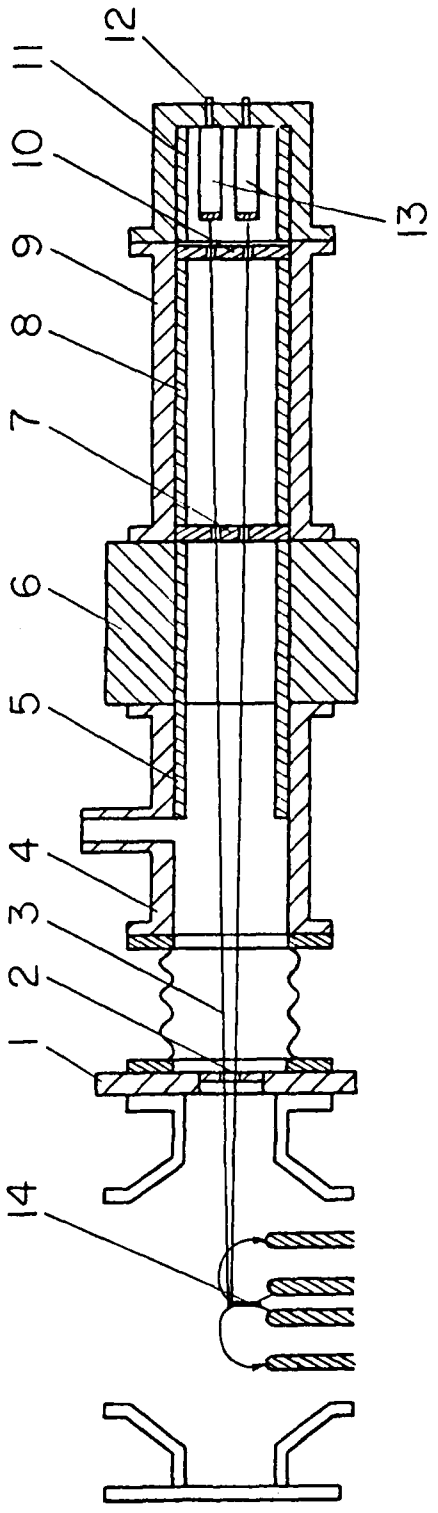

Figure 25

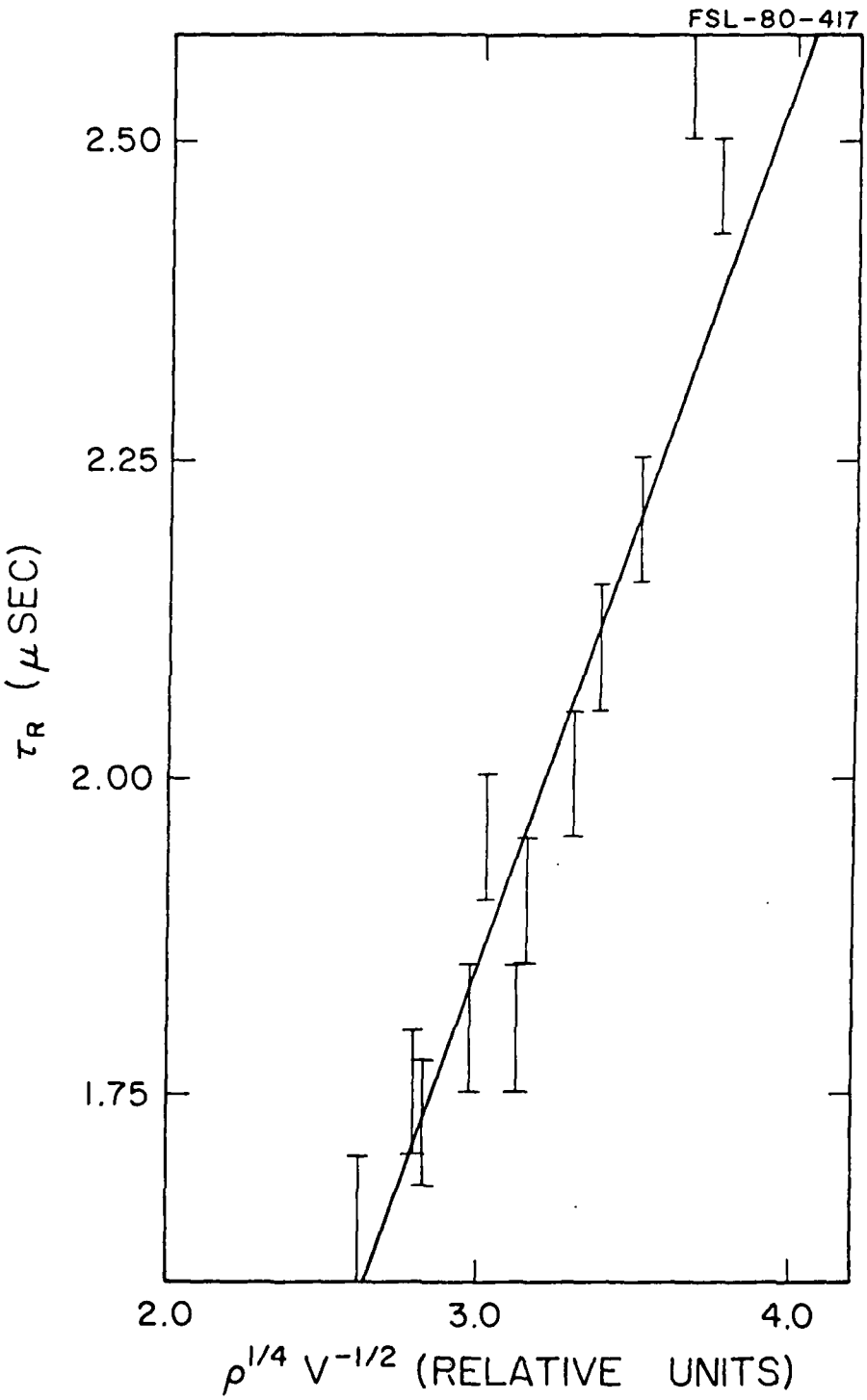
FSL-80-417
2.50
2.25
2.00
1.75
τ_R (μSEC)
2.0
3.0
4.0
$\rho^{1/4}$ $V^{-1/2}$ (RELATIVE UNITS)

Figure 26

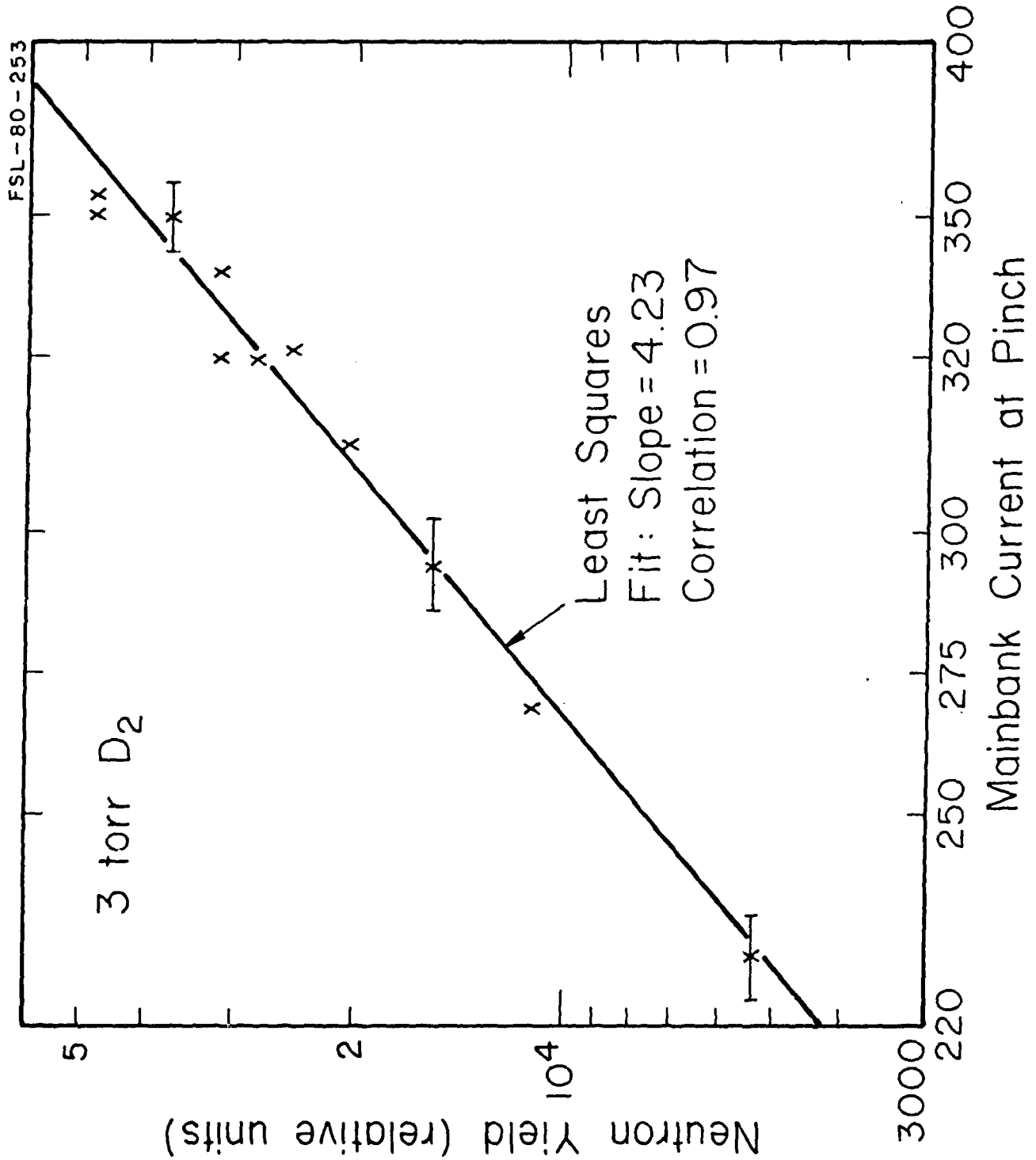
FSL-80-253
3 torr D_2
Least Squares
Fit: Slope = 4.23
Correlation = 0.97
Neutron Yield (relative units)
Mainbank Current at Pinch
5
2
10^4
3000
220
250
275
300
320
350
400

Figure 27

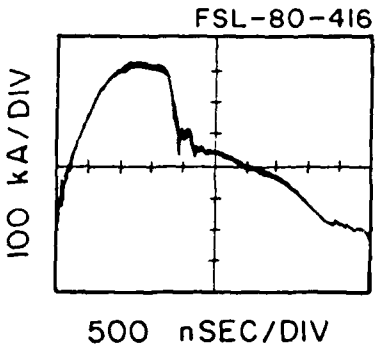

Figure 28


LMED
8